LOCKHEED
MISSILES & SPACE COMPANY, INC. • SUNNYVALE, CALIFORNIA
A SUBSIDIARY OF LOCKHEED AIRCRAFT CORPORATION

ANALYSIS OF SIMULTANEOUS SKYLAB AND GROUND BASED FLARE OBSERVATIONS

Final Summary Report
(PRELIMINARY)

by

J. L. Kulander

December, 1976

Prepared for

NASA Headquarters
Physics and Astronomy/Data Analysis
Washington D. C. 20546

Contract No. NASW-2854

Lockheed Missiles and Space Company
Palo Alto Research Laboratory
3251 Hanover Road
Palo Alto, California 94304

TABLE OF CONTENTS

ABSTRACT

		Page
I.	Introduction	1
II.	Data Reduction	5
	A. Selection of Flare	5
	B. D_3 Filtergram Data Analysis	8
	C. S082 Data Analysis	30
III.	Theoretical Analysis	43
	A. Models	43
	B. Non-Equilibrium Parameters and Optical Depths	45
	C. Electron Temperatures and Densities	68
	Appendix A - Energy Level Model	70
	Appendix B - Basic Equations	73

Analysis of Simultaneous Skylab and Ground Based Flare Observations

I. INTRODUCTION

The purpose of this program has been to reduce and analyze HeI and HeII resonance line data from Skylab and make comparison with HeI D_3 line intensities taken simultaneously from the Lockheed Rye Canyon Solar Observatory. Specifically, we will obtain relative and absolute intensities where possible as functions of position and time within the most interesting solar flare observed simultaneously from Skylab and the ground. The observed intensities will be compared with theoretical calculations made as part of this study with the objective of inferring electron temperatures and densities within the flare as a function of time.

The investigation described here has been a collaborative effort between us and the Skylab NRL principal investigating group. We would like to express our appreciation to Dr. R. Tousey for providing data before publication. Dr. J. D. Bohlin provided us with flare lists and much advice and Dr. Fred Rosenberg generously supplied tapes with microdensitometer information on many plates taken with the NRL XUV Spectroheliograph. This data is discussed in Sec. II.C.

HeI D_3 filtergrams of the solar disc were obtained from May 1973 to February 1974 at the Lockheed Rye Canyon Solar Observatory. These filtergrams contain the emission within an 0.4Å band about the center of the D_3 line (5876Å) and were taken at 15 or 30 second intervals for most of this period. The purpose of such patrol observations was to catch active

regions in early developing stages. The filtergram field of view is 8' x 10' while the spatial resolution is of the order of 1". The filtergrams thus contain a great deal more spatial information than corresponding spectrographs. The D_3 data is discussed in Sec. II.B.

Recent data show many complex and as yet unexplained phenomena in the D_3 line (Ramsey, 1970; Harvey, 1971; Ramsey, et al., 1975). The D_3 emission has shown intself to have the potential of providing significant new information on dense flare centers where its emission is generally concentrated. The following general conclusions have been drawn concerning D_3 flare structure. D_3 is observed in emission and/or absorption against the disc during most flares of importance 1 or greater. D_3 emission is generally confined to larger disc flares and occurs more frequently in limb flares. The emission component of D_3 flares corresponds to the brightest and spectrally broadest parts of the H - α flare. The localized bright centers in D_3 are much shorter lived and usually show more rapid changes than can be seen in H - α filtergrams. The brighter emission centers are visible for tens of minutes. In most cases the D_3 emission elements were adjacent to or overlying sunspots. A wide variety in flare structure has been observed.

D_3 absorption elements correspond generally to weaker parts of the H - α flare and are longer lasting than D_3 emission. The absorption components of D_3 flares aside from filaments, surges and loops, are not visible in the red wing at D_3 + 0.8Å. About half the emission components show an initial red wing brightening usually lasting for about 30 sec. This is interpreted in light of various observational evidence as an initial downward motion of the emitting region.

For purposes of comparison with Lockheed D_3 data it was decided that the NRL experiments could provide the most complete and useful complimentary information. The NRL instruments on Skylab were the extreme ultraviolet spectroheliograph (S082A) and the ultraviolet high-resolution spectrograph (S082B). The S082A instrument is a slitless spectrograph having a short wavelength range 150-335Å and a longer range 321-630Å. The images of the He resonance lines are fairly well separated, giving total integrated line intensities. S-082A images the entire solar disc for all wavelengths in rapid time sequence. The spatial resolution for the He resonance lines is estimated at 2". Time resolution depends on the exposure time, which varies from the shortest exposure of 2.5 sec. to a maximum manual exposure of 48 min. The S082B instrument also has two wavelength ranges (970-1970Å and 1940-3940Å). Spectral resolution is .04 - .08Å with a field of view of 2" x 60". There is no spatial resolution along the slit.

We have developed computer codes under the SCAP program which allow for the calculation of total He line intensities and line profiles from model flare regions. A complete description and results are given in our final summary report (Kulander, 1973) which we shall refer to as R1. These codes incorporate simultaneous solution of the line and continuum transport equations as needed together with the statistical equilibrium equations for a 30 level HeI, HeII, HeIII system. The geometrical model is a plane-parallel layer irradiated on one side by the photospheric radiation field. A statistically steady state and uniform electron temperature and density with position were assumed. The energy level model consists of all terms through principal quantum number four. Our study has been confined to conditions we believe

characteristic of He flare regions, namely electron temperatures between 10^4 and $5 \times 10^{4.6}$ K and electron densities between 10^{10} and 10^{14} cm^{-3}. Our codes also allow the solution of the statistical equilibrium equations for arbitrary values of the various line and continuum radiation fields. Results of the interpretation of the observed data in terms of these parametric solutions and with simultaneous solution of the transport equations are discussed in Sec. III.

II. A. Selection of Flare

D_3 filtergrams were taken at Lockheed during the period May 28, 1973 to Feb. 4, 1974. Generally the regions studied coincided with active regions under observation by Skylab. Photographs were taken every 15 or 30 sec. depending on seeing conditions. This data with observation times, seeing conditions, etc., is summarized in the World Data Center A Report UAG-43, Coffee, 1975.

A list of flares observed by the NRL S082A instrument was compiled by J. D. Bohlin and V. E. Scherrer and generously supplied to us by Dr. Bohlin. This list is given in Table II.A.1. A total of 17 flares was observed, of which about a dozen had reasonably complete coverage. The list is a result of the merging of flare logs compiled independently from two different approaches. One log was made from a plate-by-plate inspection of the entire mission, using as a criterion whether or not He II 304 was solarized and the presence of emission lines from the high stages of ionization (primarily in the short wavelength band). The other log was compiled by comparing S082A coverage with the SOLRAD data.

Of these 17 flare events we have simultaneous D_3 coverage for only 7. These are the flares of 15 June 73, 7 Aug. 73, 9 Aug. 73, 31 Aug. 73, 1 Sept. 73, 5 Sept. 73, and 7 Sept. 73. Our films for these seven flares were studied in detail. For two of these events only two frames were taken by S082A. Since as we shall see shortly several exposures at each time are normally required for good intensities, these events would not yield much time dependent information. The 15 June 73 event occurred very early in the morning in Los Angeles and our D_3 data is of very poor quality. The 1 Sept. event is very close to the limb and the contrast is poor on our film. The 5 Sept. event shows minor activity in D_3 and our coverage does not begin until after the maximum. For the 7 Sept. event neither NRL nor Lockneed has coverage at flare maximum.

Thus the most promising event where there is both S082A and D_3 coverage through the flare maximum is that of 9 Aug. 73. Flare maximum is near 15:53 UT. NRL has 14 frames between 15:20 and 15:58 while we have D_3 filtergrams every 30 secs. under good seeing conditions.

TABLE II.A.1

NRL S082A FLARE LIST

Date	NRL Plate Nos.	Time (UT)	Position Angle ($\pm 5^{\circ}$)	Notes
15 June 1973	1A312-347	14:11-14:38	N20W45	WV LG & ST. M2: Max. 14:14. Complete sequence.
7 Aug. 1973	2A006-007	18:47 18:49	N10W30	C3: Max. 18:47. Both plates LG WV. Many flare images superposed on film defect. Exposure one hour earlier and later still show AR to be very bright.
9 Aug. 1973	2A022-035	15:20-15:58	N10W50	M2: Max. 15:53. May be sequence of two flares, with small limb flare on 2A022 the cause of large EPL. Many flare images superposed on film holder defect.
31 Aug. 1973	2A356-357	21:57 21:59	S05W15	Two exp. (WV ST) of small flare. Emission lines well-separated and compact.
1 Sept. 1973	2A371-373	21:26-21:32	N05E80	Subflare. Emission lines not distinct. LG & ST WV. Max. 21:15.
2 Sept. 1973	2A376	00:46	S10E70	Subflare. Emission lines not distinct. ST WV. Max. 00:43
4 Sept. 1973	2A398-399	11:29-11:32	S20E70	Twin solarized spots in He II. Bright footpoints in many highly ionized lines WV LG & ST, synoptic pair. Max. 11:30
4 Sept. 1973	2A403	16:36	N10E10	C6: Max. 16:35
5 Sept. 1973	2A419-420	18:31-18:37	Disk Center	Distince arch visible ST WV only.
5 Sept. 1973	2A421-422	20:15-20:20	S20W30	Max. @ 20:10. Small flare in NE quadrant. Complex emission structure
7 Sept. 1973	2A432-448	12:21-18:28	S20W50	X1 flare w/4 consecutive peaks. Post flare loops over neutral lines esp. apparent. AL1 ST WV. Max. 12:10.

Date	NRL Plate Nos.	Time (UT)	Position Angle ($\pm 5^{\circ}$)	Notes
10 Sept.1973	2A459-460	02:32	S20W60	Synoptic pair may have caught small flare. He II barely solarized. LG & ST WV.
2 Dec. 1973	3A037-045	15:04-15:17	S10W80	M1 flare. Max. 15:18 LG & ST WV. Good sequence.
16-17 Dec.73	3A097-143	19:00-02:00	S20E85	Complete sequence on C2 & M1 (Max. 00:32 & 00:41) limb flares. 47 plates total.
22 Dec. 1973	3A176-178	00:22 01:20	S10E05	Small flare on 3A176 (ST WV); emission lines still apparent on synoptic pair 177 & 178. May only be a very bright AR.
15 Jan. 1974	3A375-376	14:25-14:28	N10W85	Limb flare (C6: Max. 14:25) with sheet-like surge. ST WV only. Surge seen hour earlier as well.
21-22 Jan. 74	3A452-472	23:15-00:49	N30W50	C8 flare, full sequence of 21 plates. Max. 23:23.

II. B. D_3 Filtergram Data Analysis

The flare event of 9 August 73 occurred in the active region designated 185 (NW quadrant) on the NOAA daily charts. Fig. II.B.1 shows the NOAA schematic of the Sun at 14:20 UT. The region was observed in the D_3 line at Rye Canyon for several days before and after the flare. As originally observed the spot group was very complex with many small and intermediate size spots. By 9 August only the largest spot and one of the smaller eastern spots remained. The spot centers are about 1-1/2' apart and are located roughly at position angle N 10^{o}, W 50^{o}. The smaller spot lies roughly E of the larger one. The central intensity of the larger spot is as low as 35% of the continuum while in the smaller spot it is about 75%.

Figs. II.B.2, 3, and 4 are photographs of the spot region through the D_3 filter at 15:46:00, 15:53:30 and 15:57:00. Exposure times were a small fraction of a sec. The first photograph shows the pre-flare undisturbed environment, the second photograph the maximum and the third photograph the decay phase. The W limb is visible in each exposure.

The flare or flares occur in the smaller easterly spot. Visual inspection of the film shows two distinct bright emission points on each side of this spot. These two bright flare kernels can best be seen in Fig. II.B.3 at 15:53:30. Both kernels lie roughly in a N - S line. The northern kernel is first visible at 15:52 fading out at 15:58 while the southern kernel is first visible at 15:53 and fades out at about 15:57. Both kernels appear very bright against the spot background. They appear to represent two distinct events at different locations.

Two sequences of densitometer tracings have been made from our original 8-mm film. The first consists of tracings of the four best coincident frames listed in Table II.C.2 at 15:46:00, 15:53:30, 15:54:00, and 15:57:00. The slit size used was 8 x 8 microns. Digital output for intensity was obtained using our H&D curves for 80 x 80 micron and 32 x 32 micron averages. 32 microns corresponds to 1.0" arc. The area traced was 106" x 160" and is shown in Fig. II.B.1. Figs. II.B.5 and 6 show intensity contours of the smaller spot from the tracings at 15:46:00 and 15:53:30. The two distinct emission areas are prominent at 15:53:30. The area covered by the Figs. is 25" x 30". The contours are labeled with the percentage of the continuum intensity.

Fig. II.B.1.

NOAA SCHEMATIC OF THE SUN FOR AUG 9, 1973 AT 1420 UT

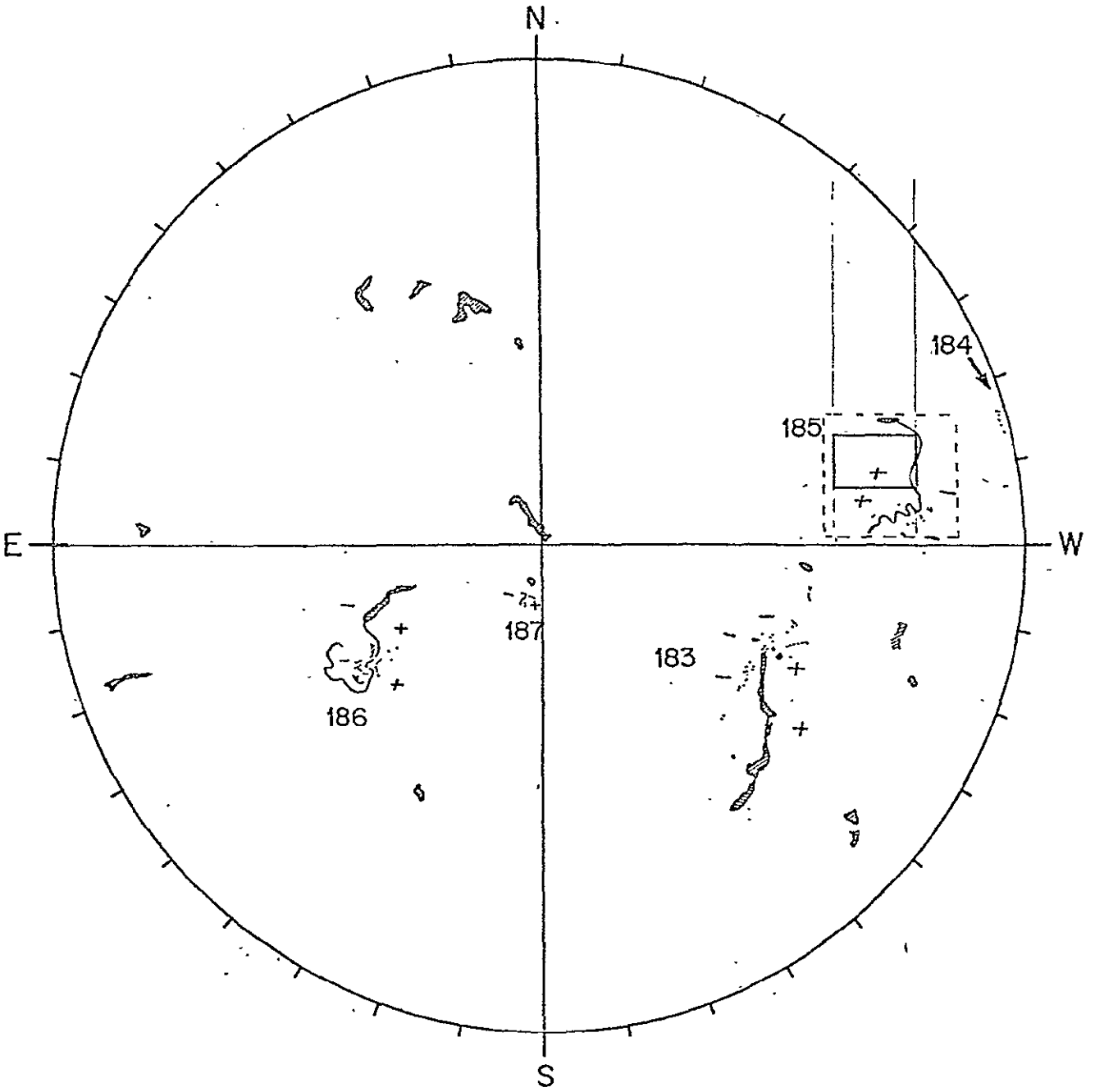

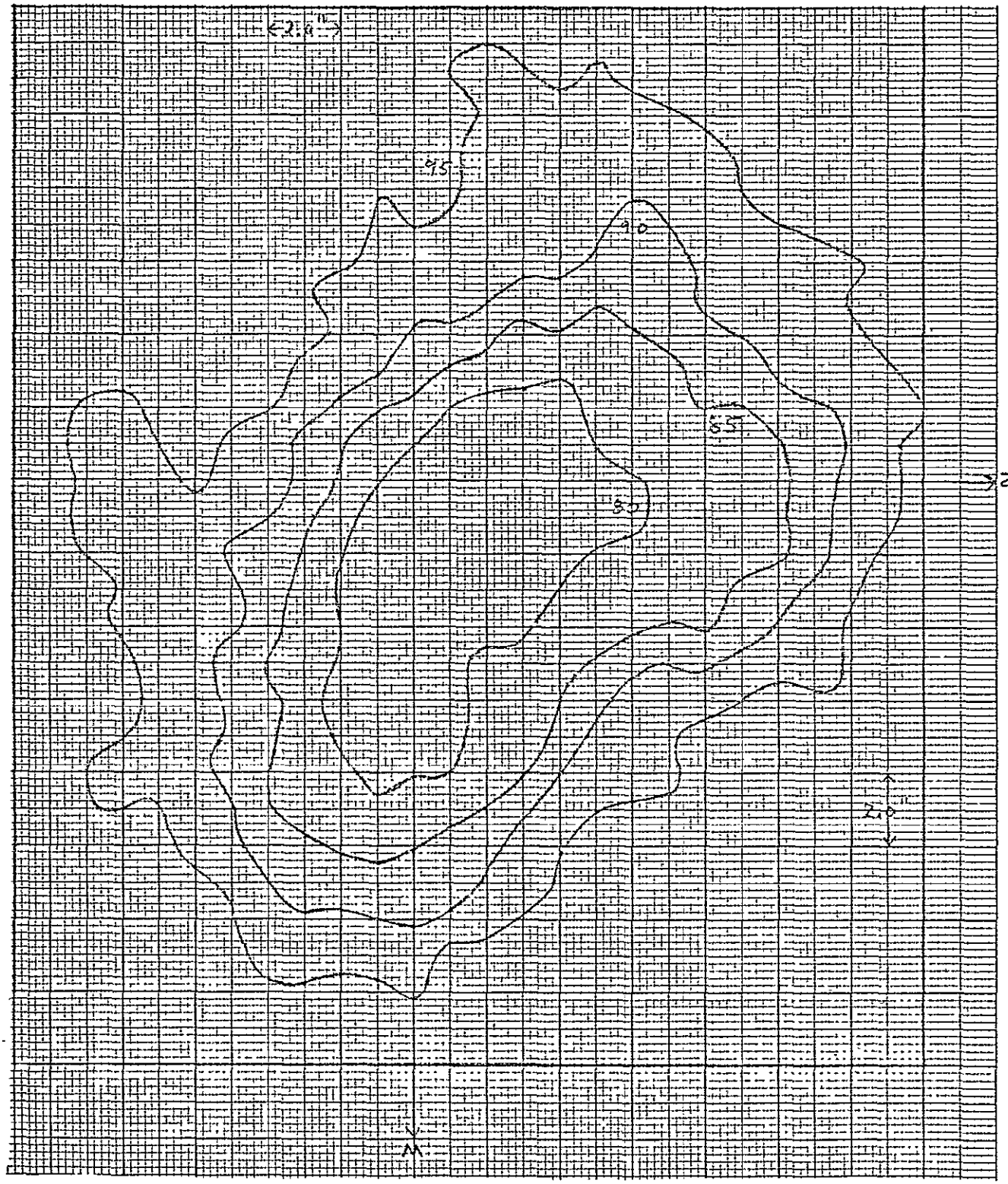

Figure II.B.5 D_3 Filtergram Intensities in Percent of Normal Continuum.
UT 15:46:00
Area 25" x 29"

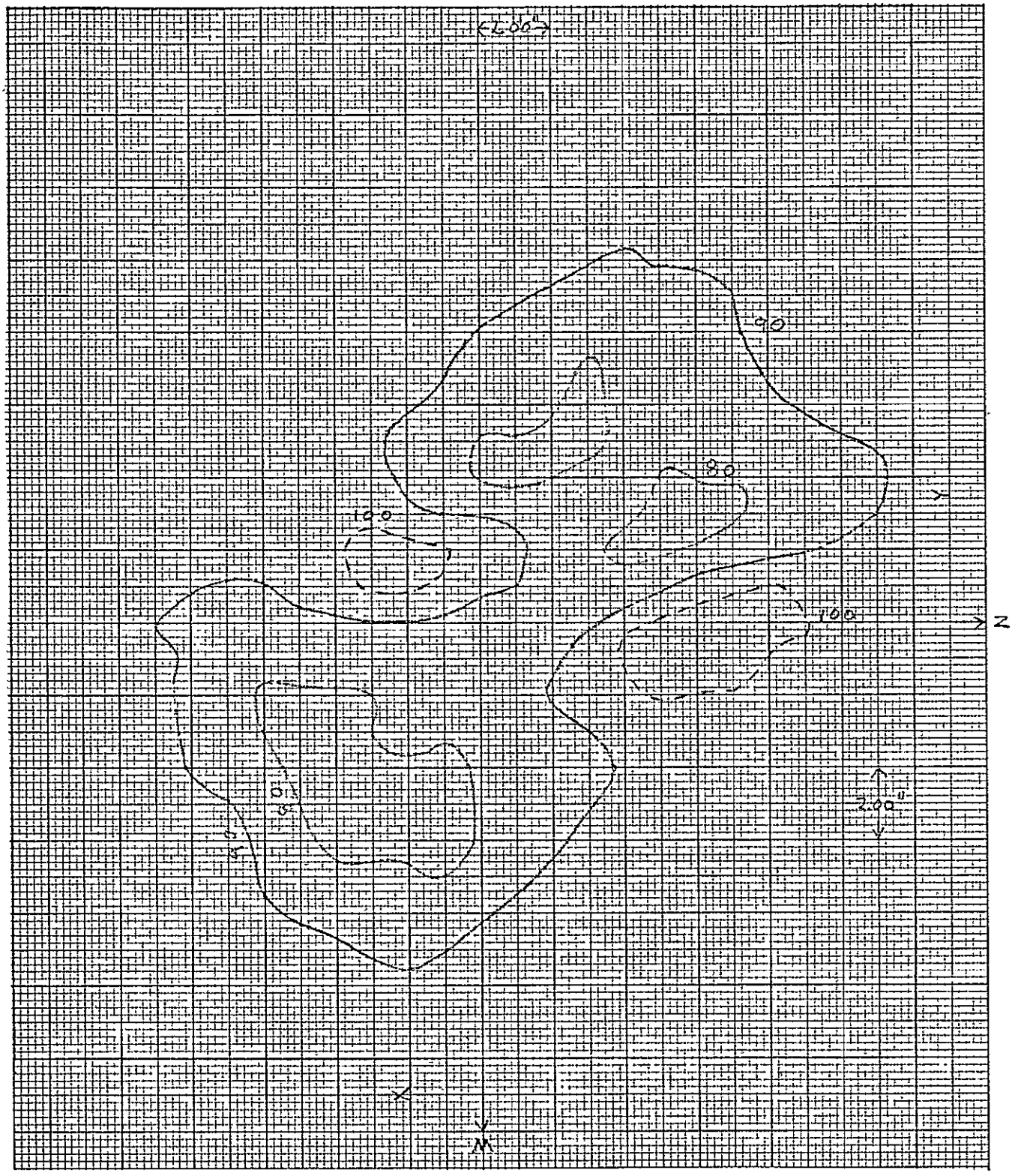

Figure II.B.6 D_3 Filtergram Intensities in Percent of Normal Continuum.
UT 15:53:30
Area 25" x 29"

The second sequence of tracings represents a similar area for each of the twelve frames taken every 30 sec. between 15:51:00 and 15"56"50 UT. The slit size used at this time was 24 x 24 microns or 0.75". Intensity contours for these frames are shown in Figs. II.B.7 to II.B.18. The time and average background intensity are given on each figure. The contours represent 360, 400, 440, 480 and 520 arbitrary intensity units. Each figure shows an area of approximately 23" x 34". The contours are labeled with the relative intensity values. The N and W direction is indicated on each figure. Areas within the spot with intensities greater than the normal continuum are shown on a number of the frames. There appear to be many instances of very small bright emission points that last for only one frame, see for instance Figure II.B.8. The southern flare kernel is first seen at 15:52:00 with the northern flare kernel beginning at 15:52:30. This is followed at 15"53"00 by a slight diminishing in intensity in both flares (possibly due to the initial red shifting noted by Ramsey, 1975) followed by the greatest intensities at 15:53:30 in the northern flare.

The northern flare becomes much more intense than the sourthern flare. The maximum intensity at any one point relative to the undisturbed continuum is 1.26 in the northern kernel and 1.10 in the southern kernel. With respect to the underlying spot backgrounds these maximum relative intensities become 1.62 and 1.42. The area of the northern region becomes much larger at maximum while that of the southern region remains about the same. The intensities in both regions slowly decay still being slightly above background at 15:56:30. These features are illustrated in Figs. II.B. 19 and 20 where we show the intensities at four different locations within the flare for each frame relative to the initial spot intensity at that location.

We note the rapid rise to maximum followed by the slower decay. The southern kernel reaches maximum intensity at 15:52:00. In bothflares there seems to be an oscillation in intensities with a period of 1 - 1-1/2 minutes.

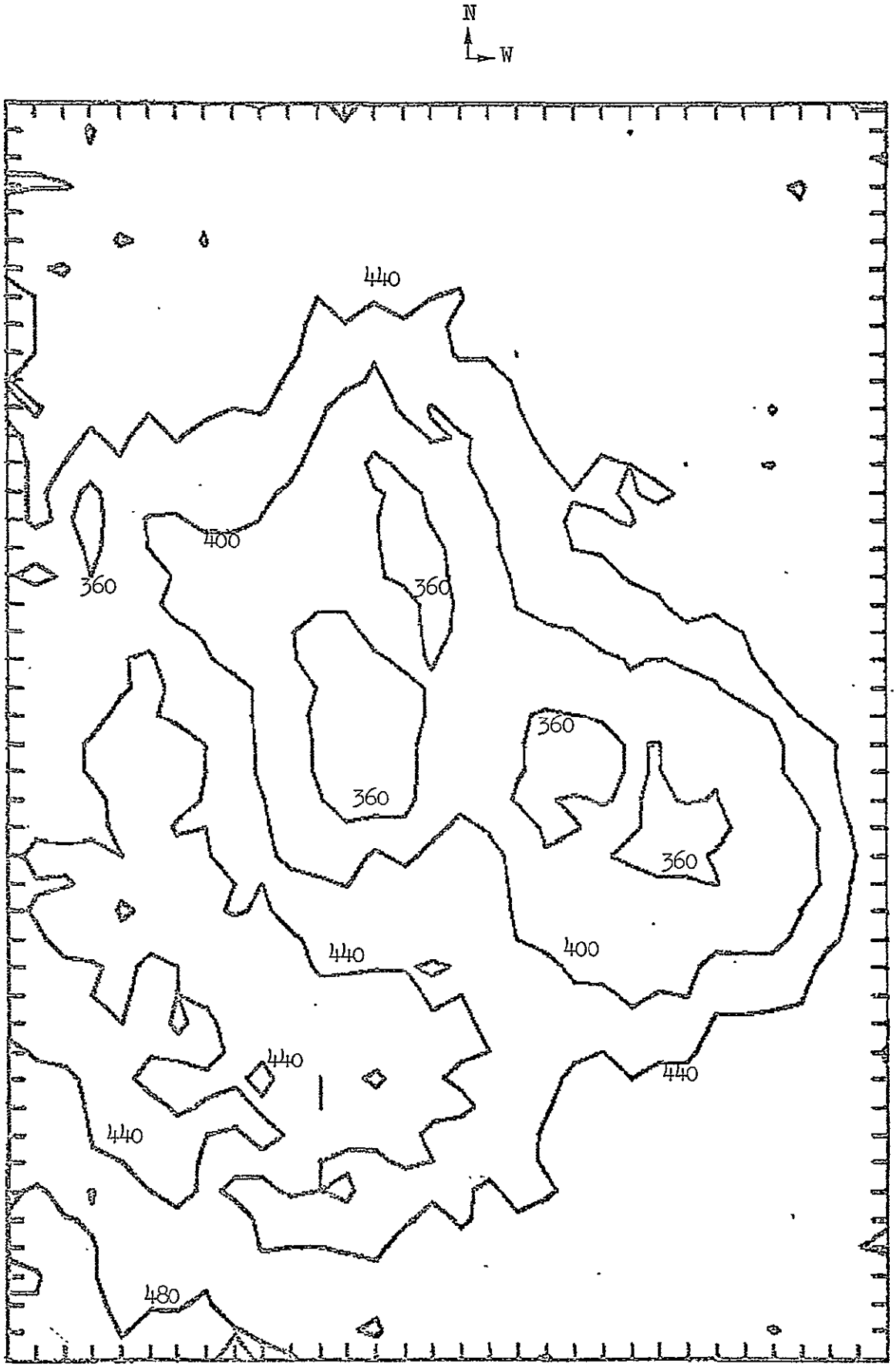

Figure II.B.7 Relative D_3 Filtergram Intensities.

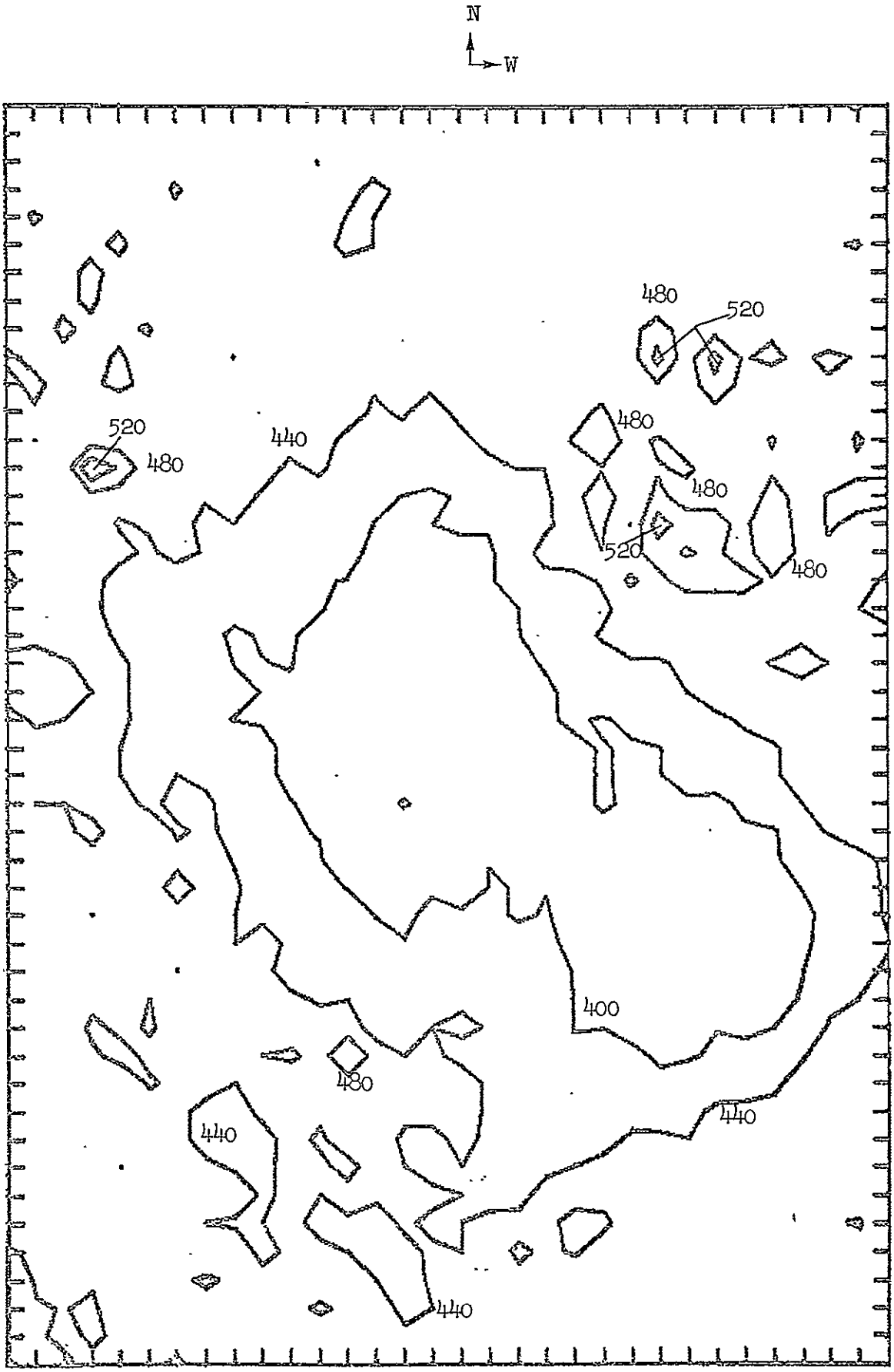

Figure II.B.8 Relative D_3 Filtergram Intensities.

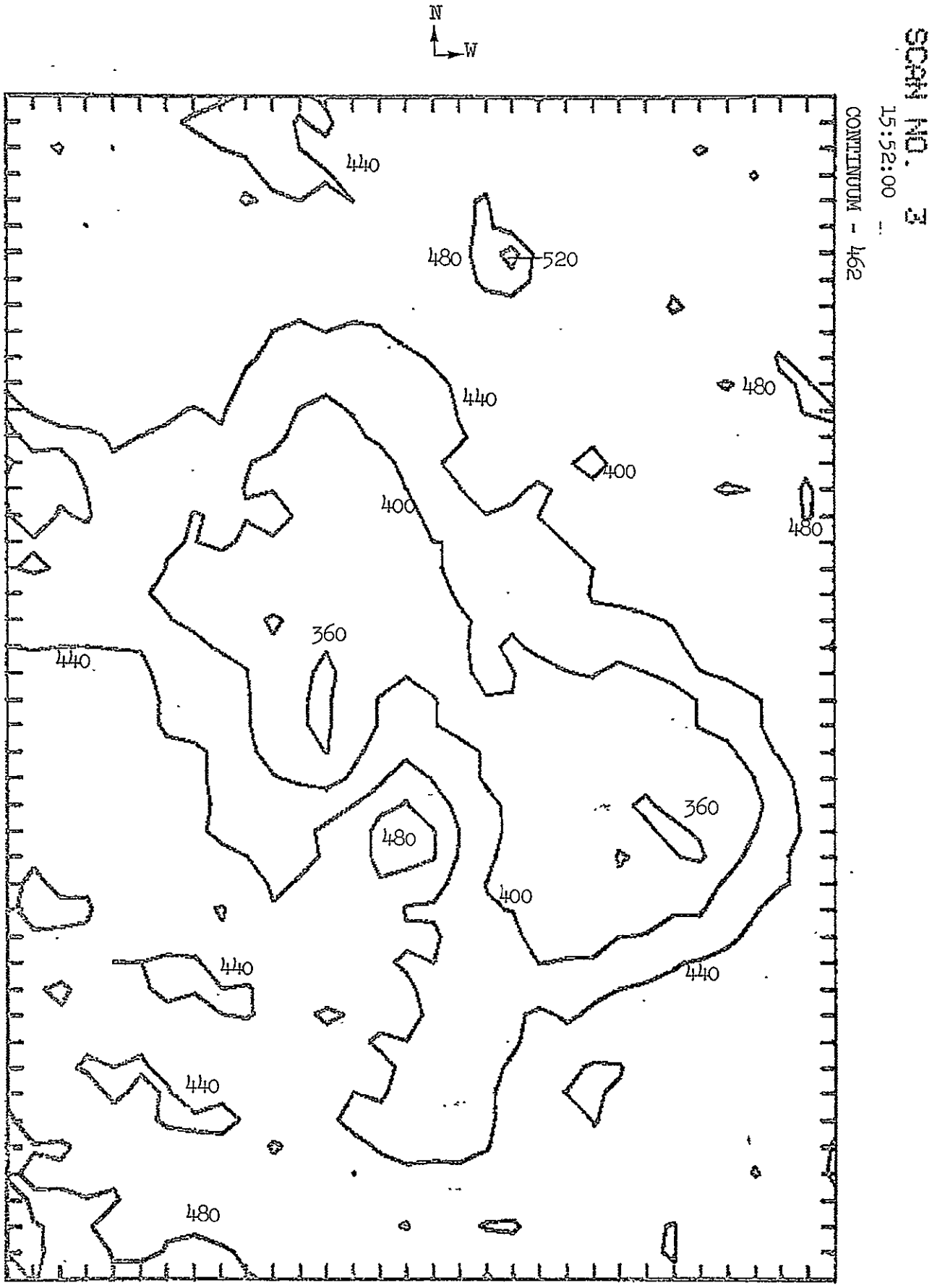

Figure II.B.9 Relative D_3 Filtergram Intensities.

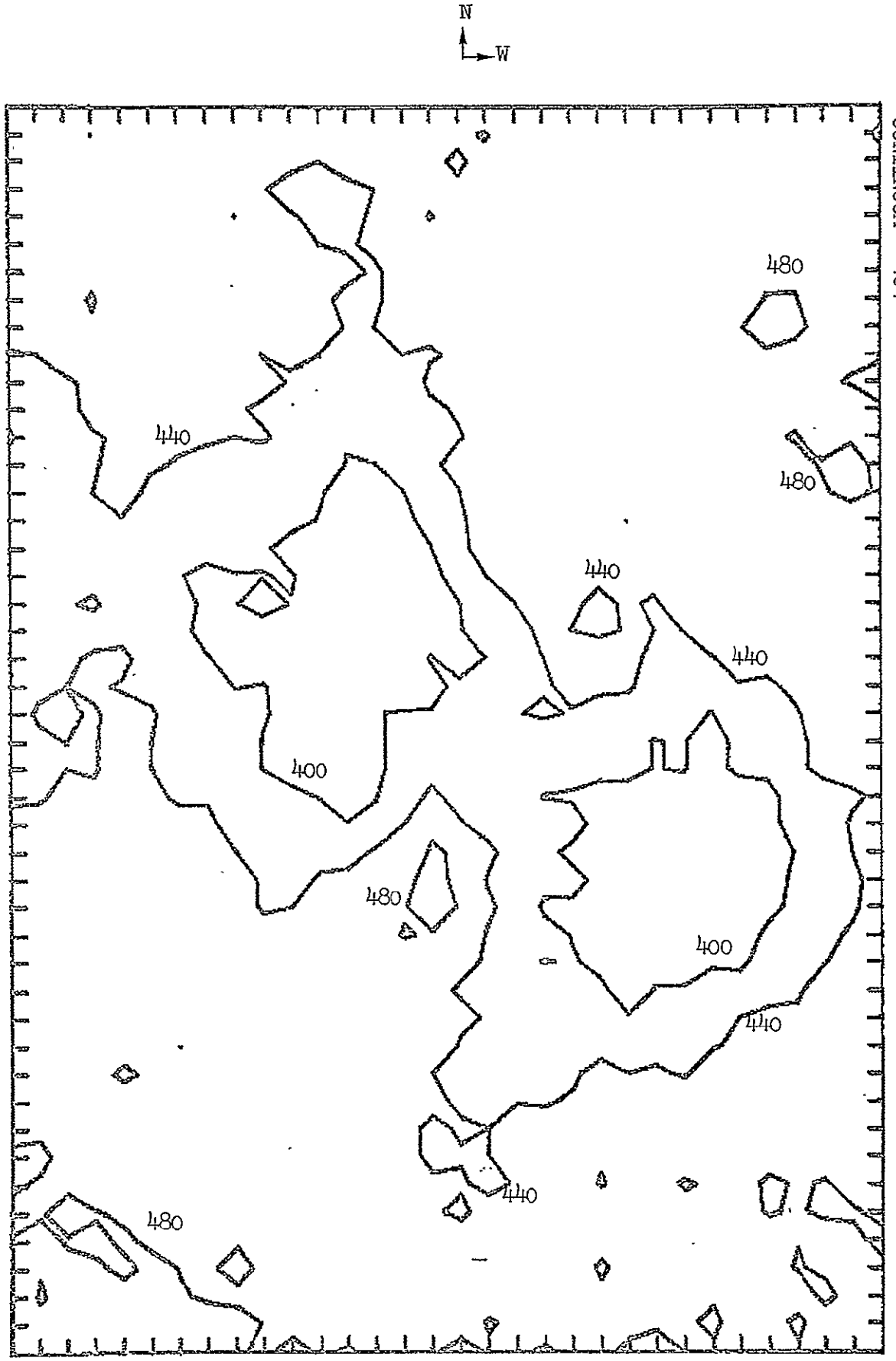

Figure II.B.10 Relative D_3 Filtergram Intensities.

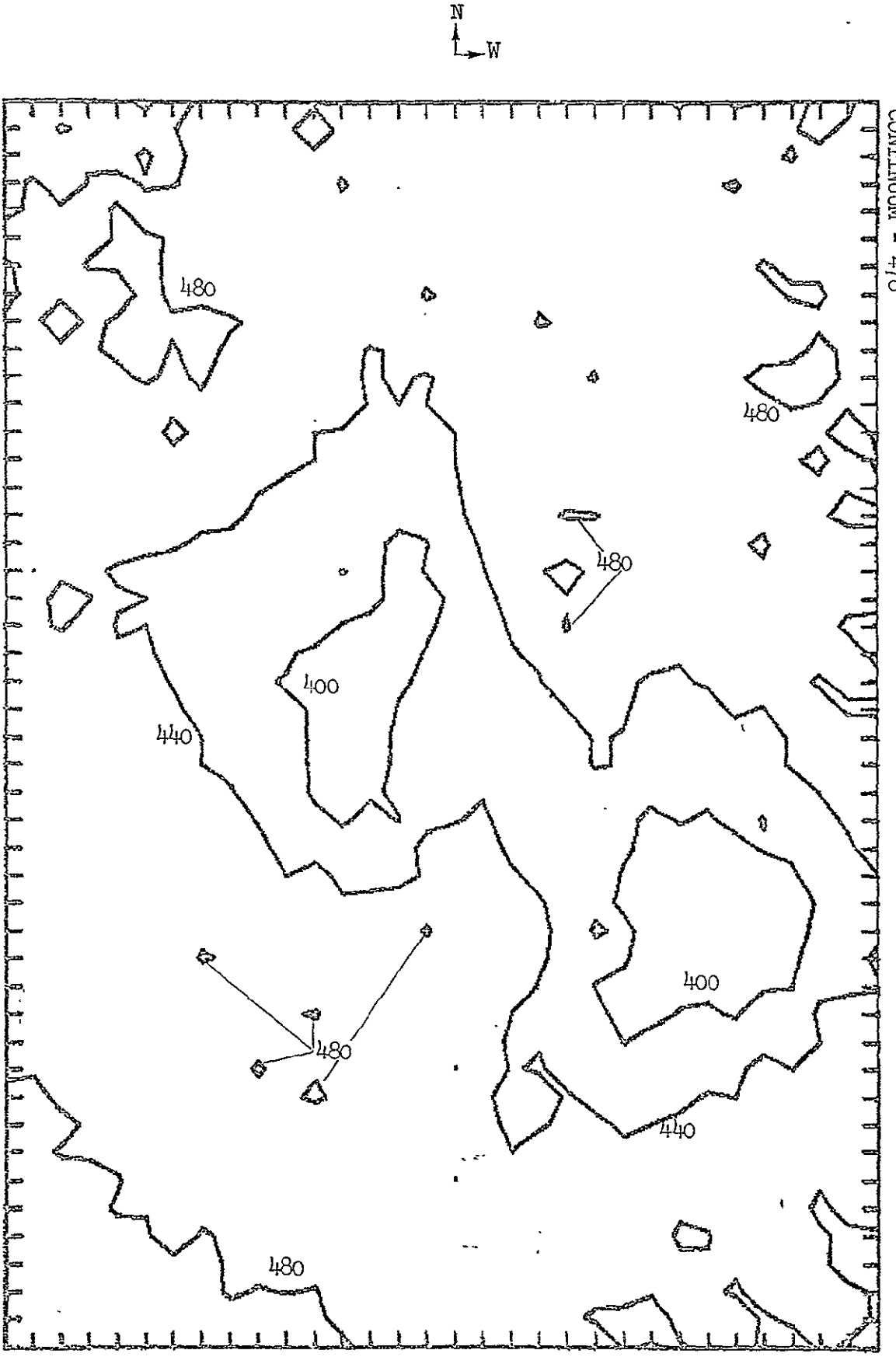

OCT 10, 5
15:53:00
CONTINUUM - 476

Figure II.B.11 Relative D_3 Filtergram Intensities.

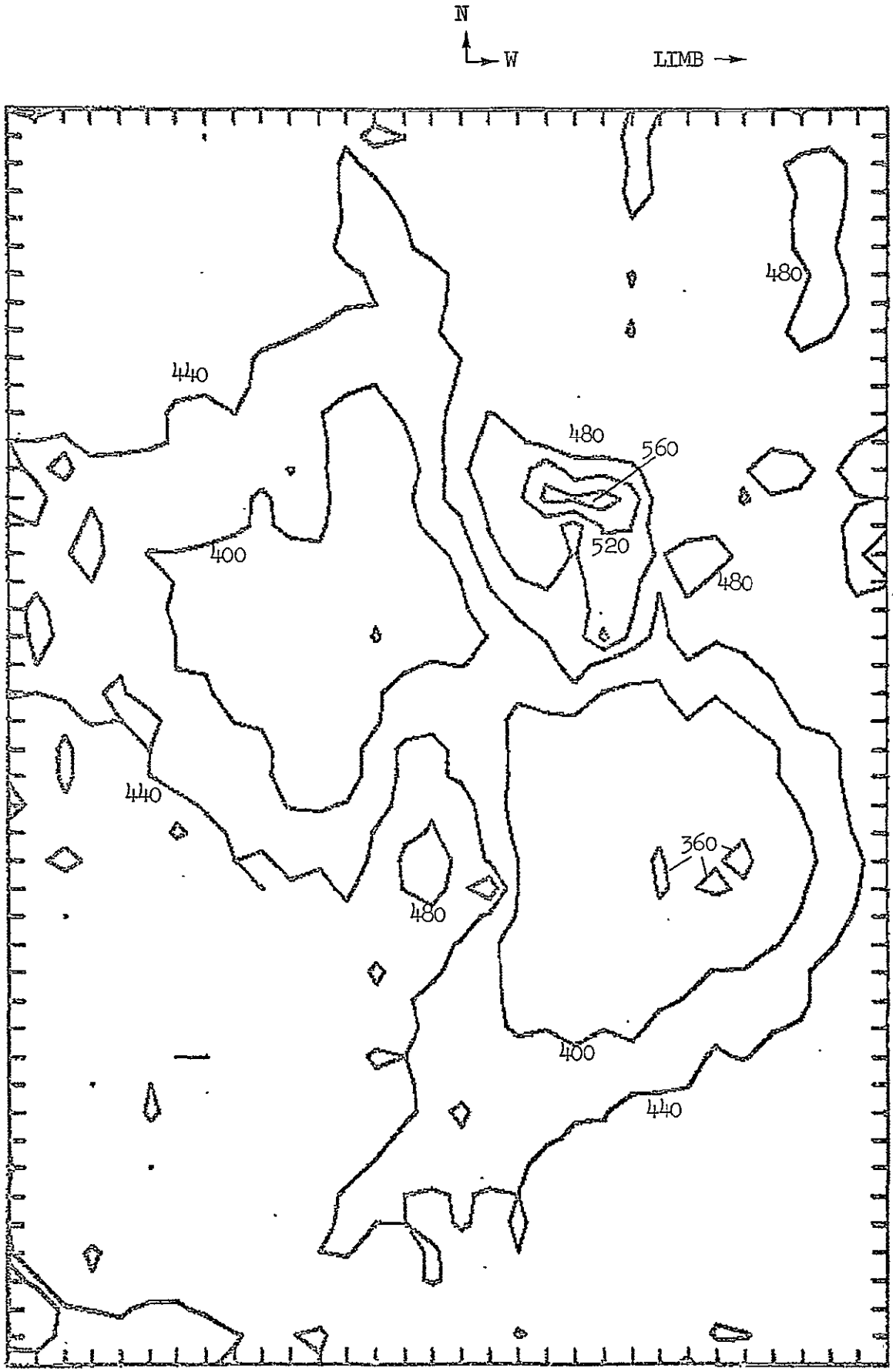

Figure II.B.12 Relative D_3 Filtergram Intensities.

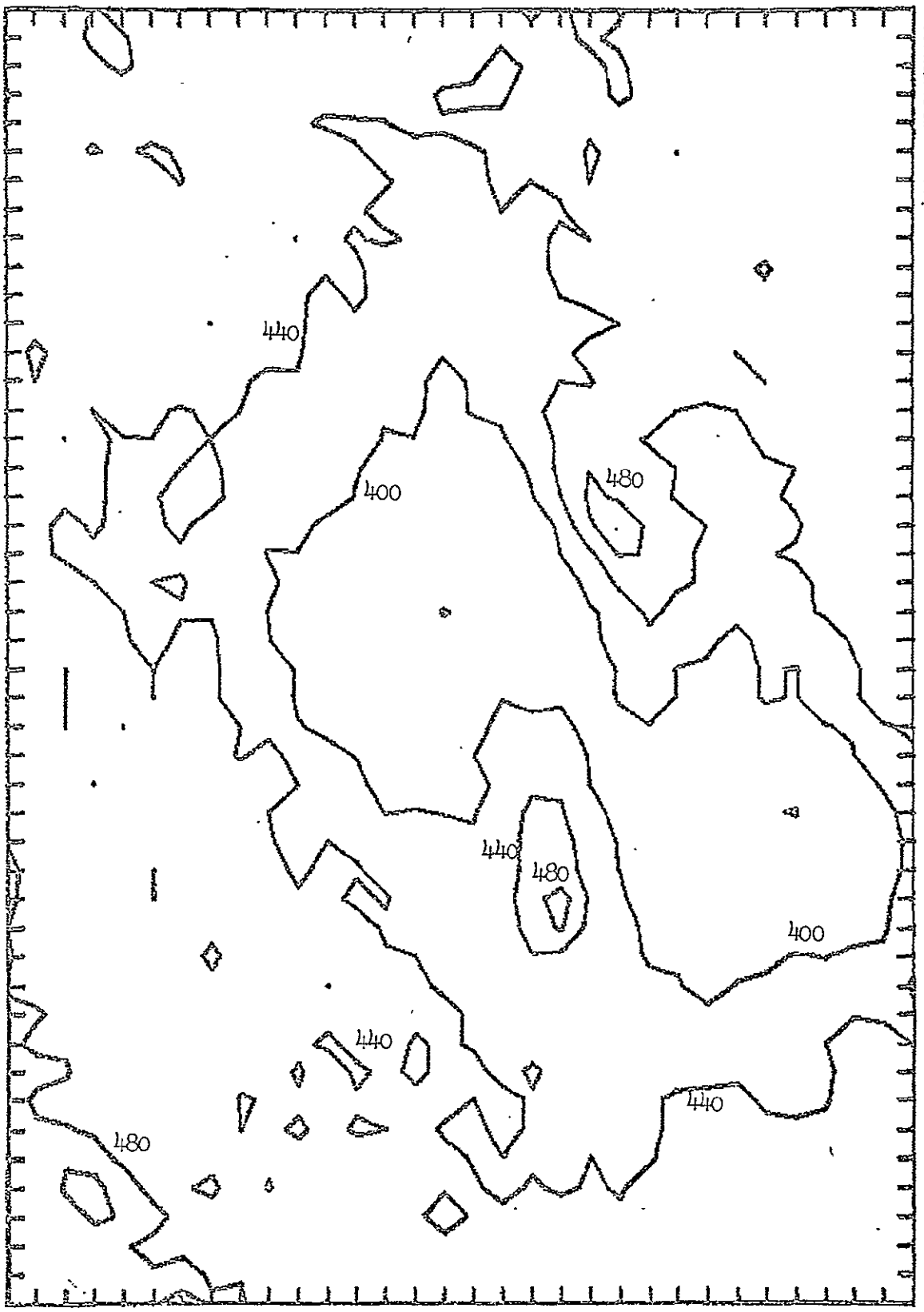

Figure II.B.13 Relative D_3 Filtergram Intensities.

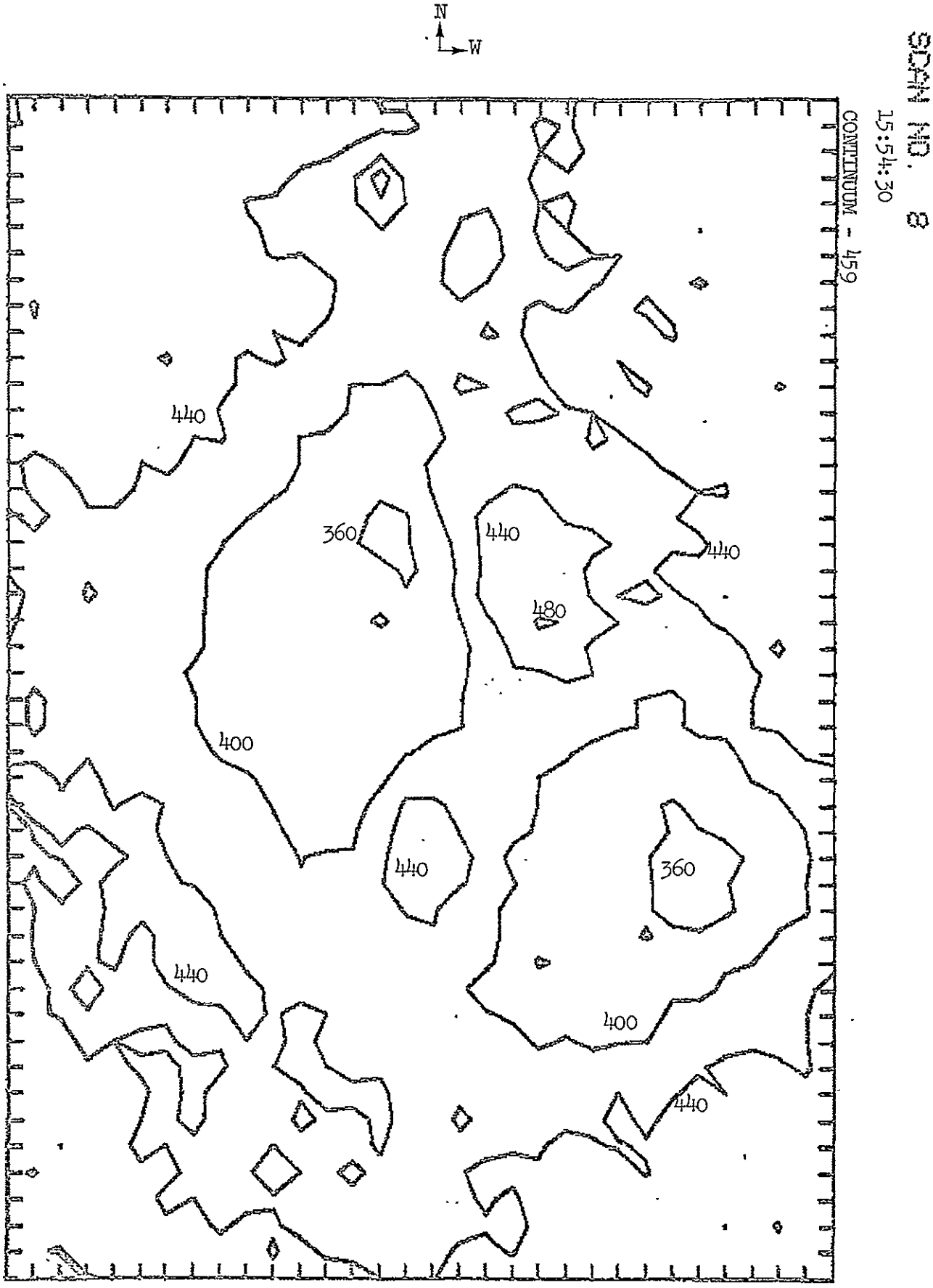

Figure II.B.14 Relative D_3 Filtergram Intensities.

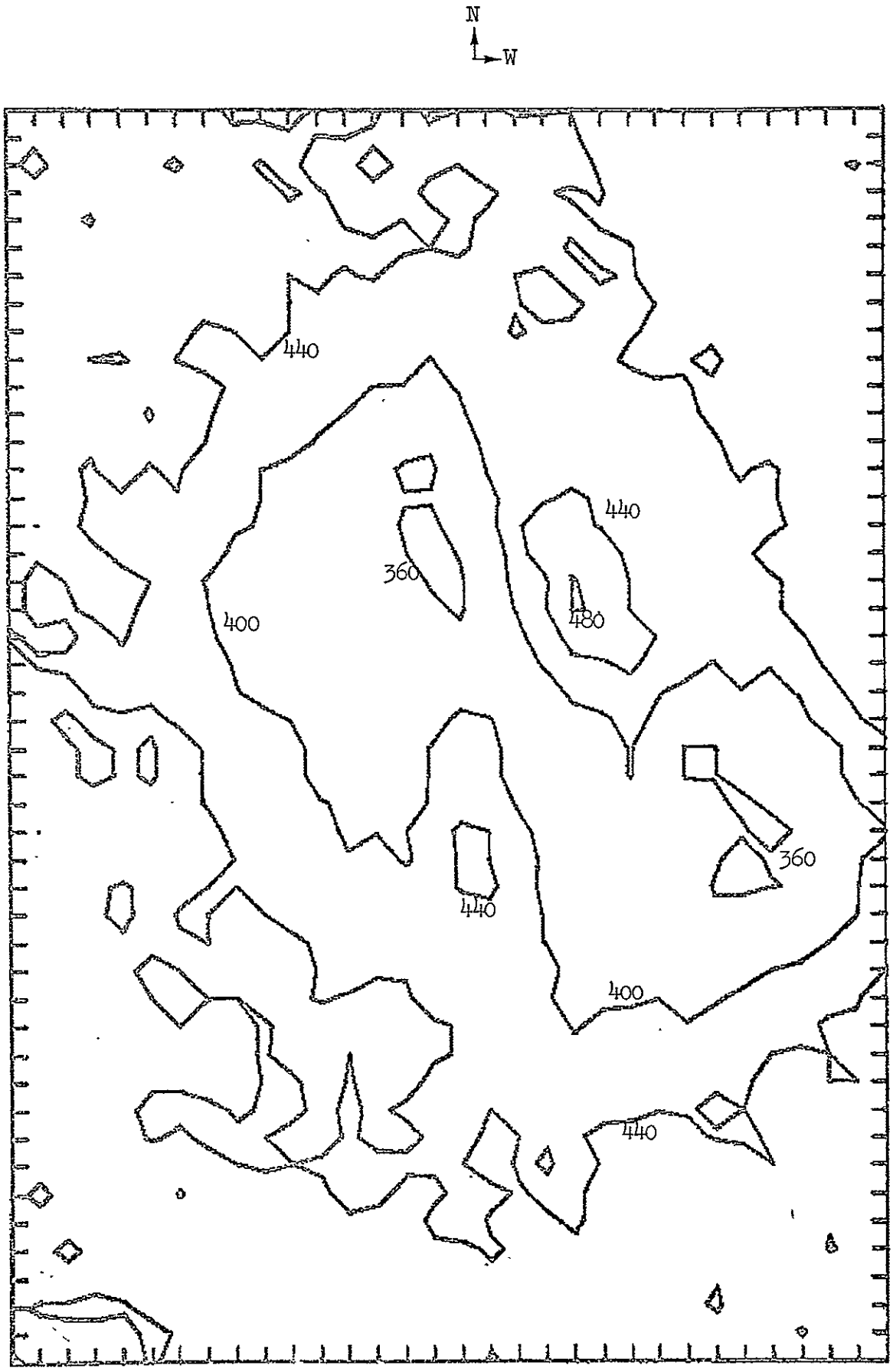

Figure II.B.15 Relative D_3 Filtergram Intensities.

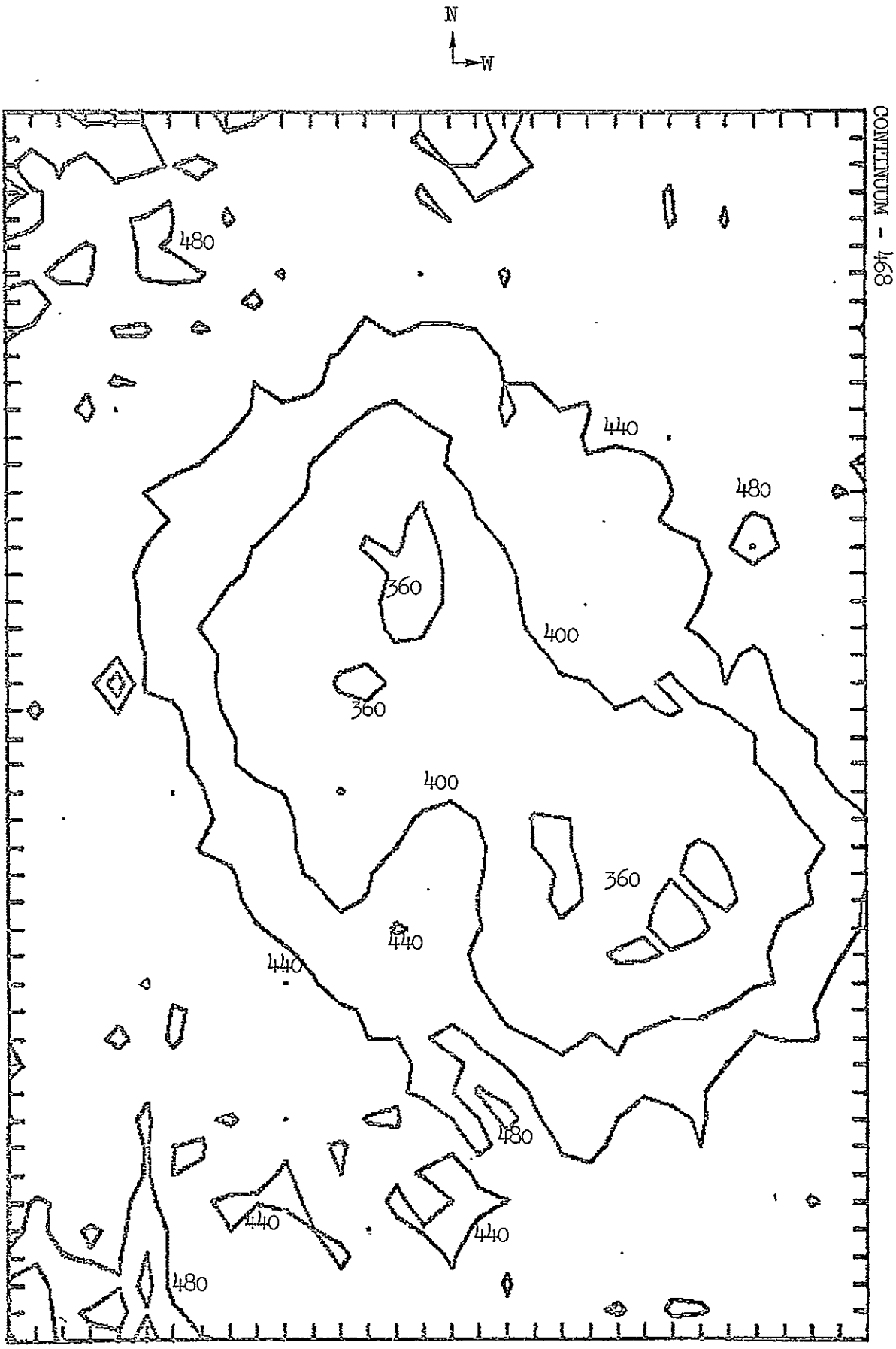

Figure II.B.16 Relative D_3 Filtergram Intensities.

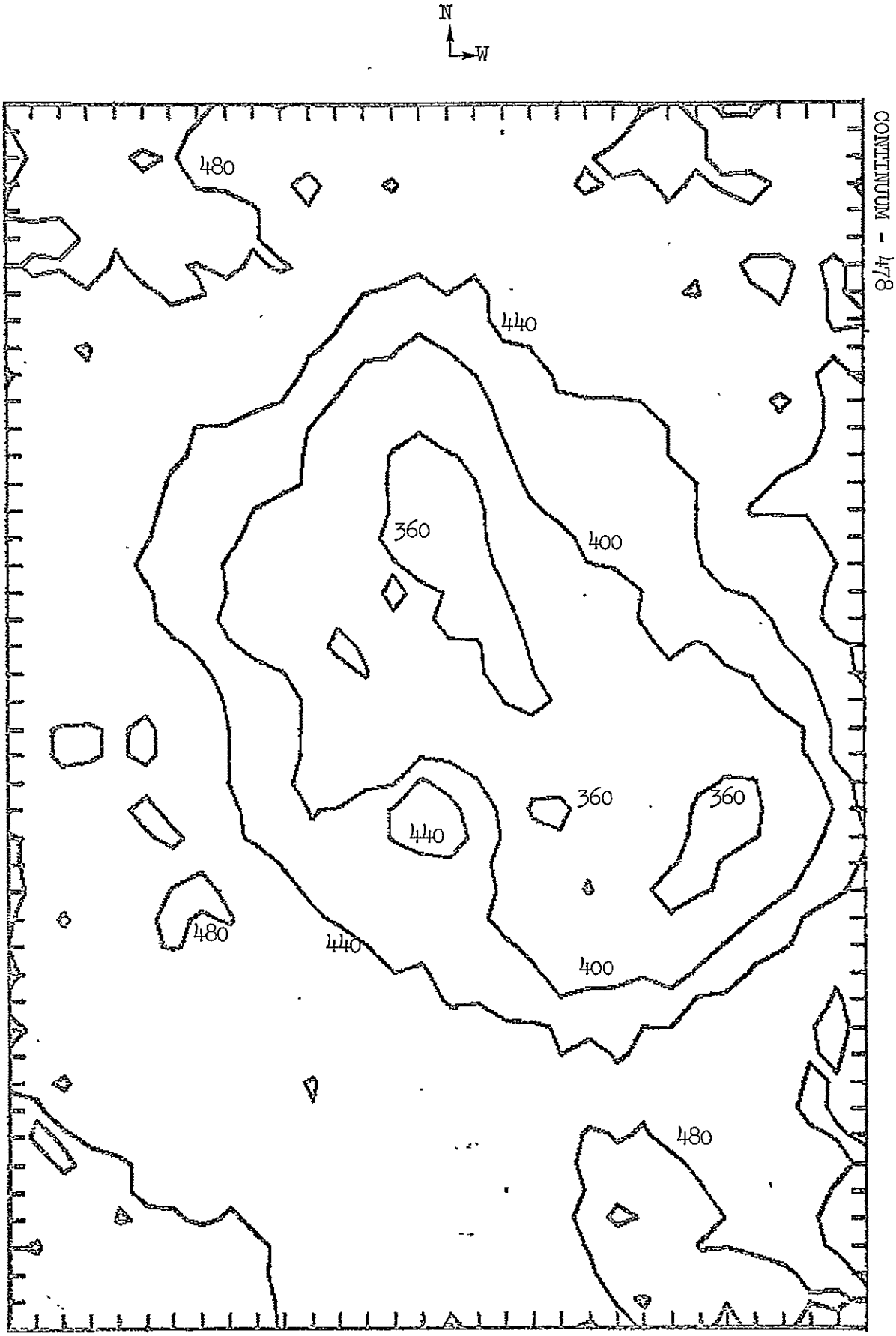

Figure II.B.17 Relative D_3 Filtergram Intensities.

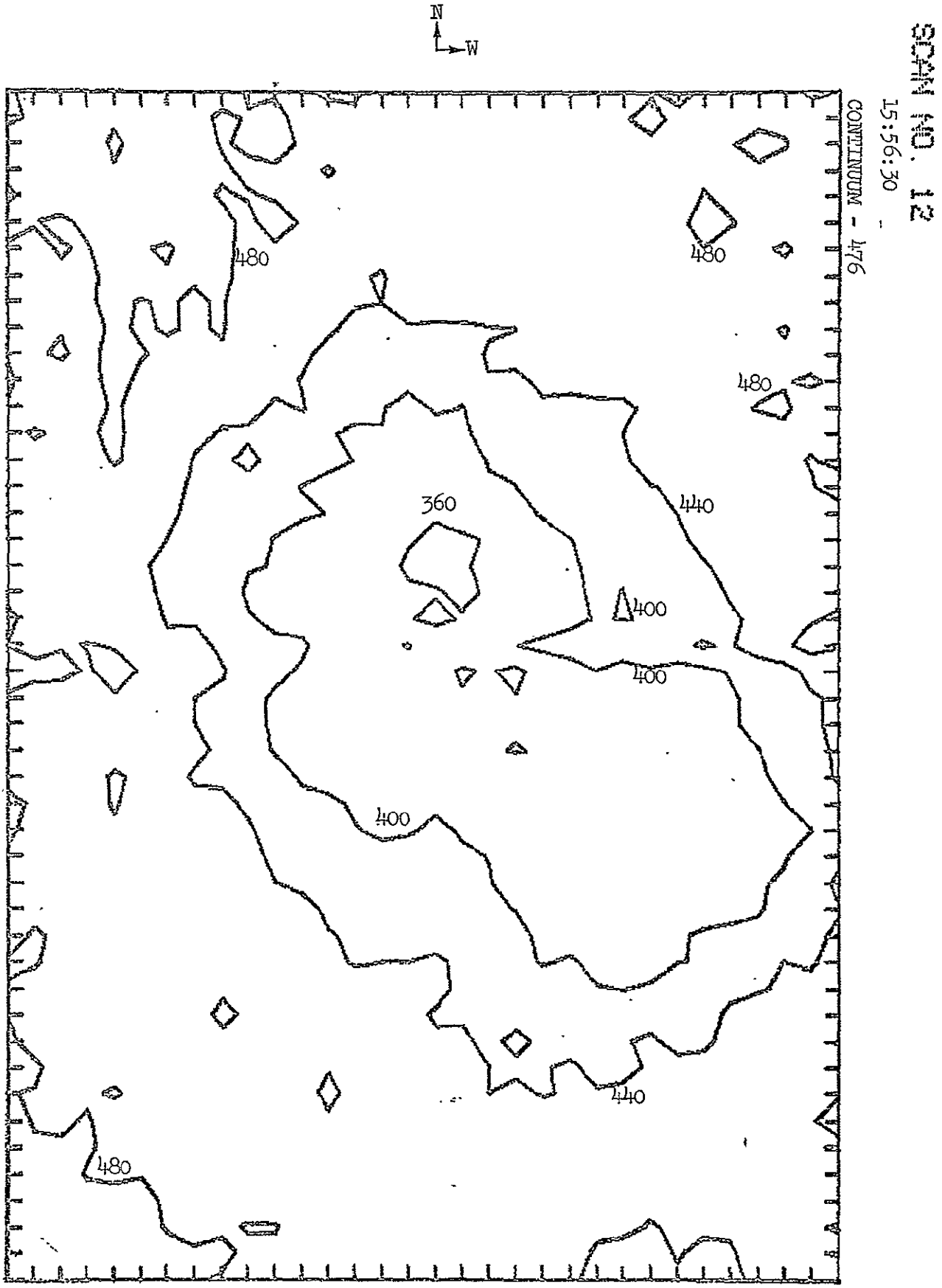

Figure II.B.18 Relative D_3 Filtergram Intensities.

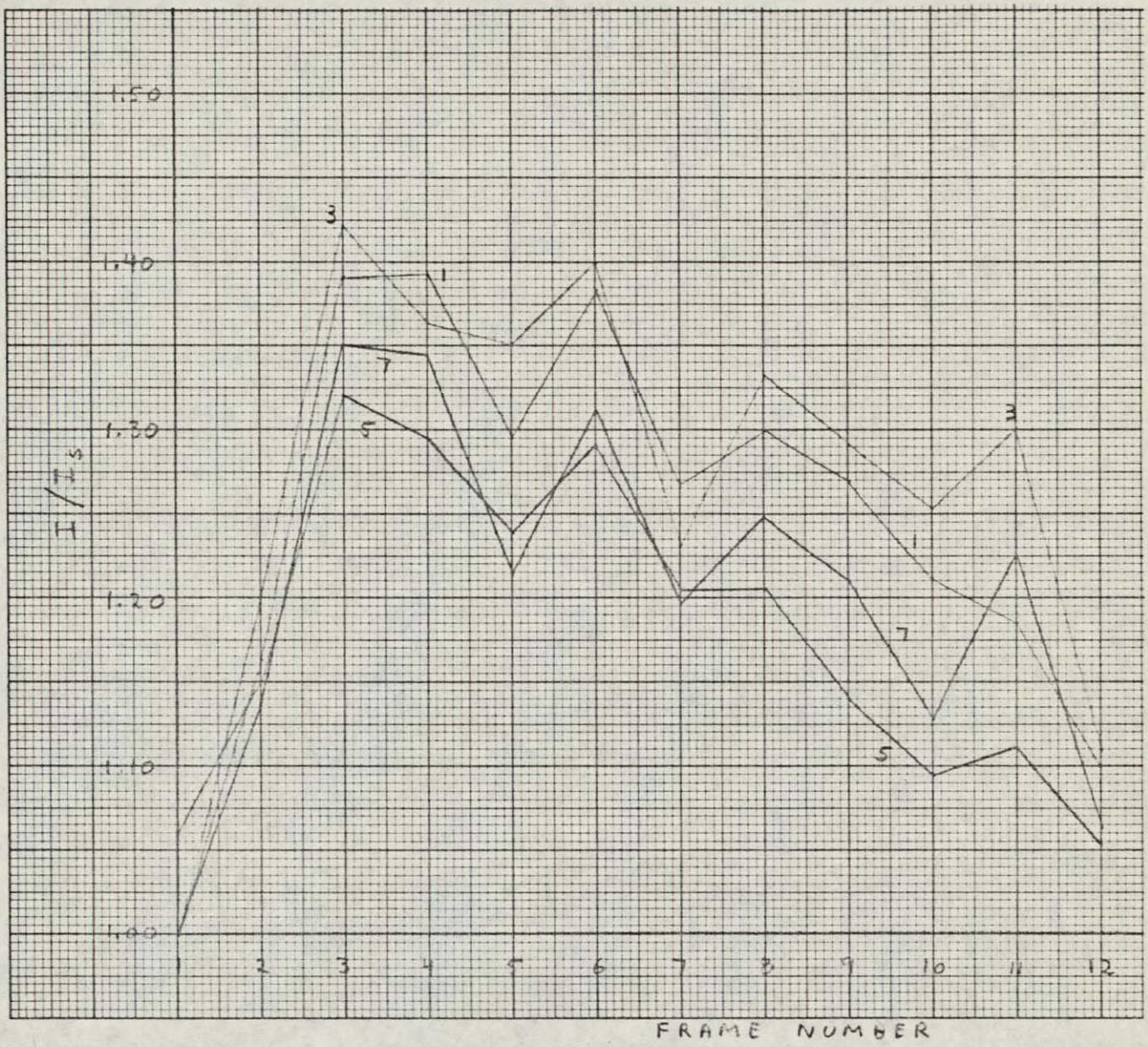

Figure II.B.19 D_3 Intensities Relative to Underlying Spot Background for 4 Positions in South Flare Kernel.

II. C. S082 Data Analysis

A list of the 14 NRL plates for the flare of 9 Aug. 73 is given in Table II.C.1 along with exposure times, wavelength range covered, and comments. We can see that only the four plates 23, 29, 30, and 31 encompass the wavelength range for the resonance lines of HeI, i.e., the long wavelength range. Plate 23 is vastly overexposed while we note that on plates 29, 30, and 31 the 584 Å line is so badly out of focus as to render quantitative analysis impossible. The longer exposures on the short wavelength plates give a solarized flare kernel at 304 Å limiting analysis to exposures of 10 sec. or less. Plate 32 is fogged due to pressure of the backing plate against the film. The usable plates for our purposes are then 24 - 27, 33, and 34. These plates will only provide information on the resonance lines of HeII.

Since plates 26 and 27 and plates 33 and 34 are taken at essentially the same time we chose the shorter exposure time plates 26 and 34 for analysis. The four most useful frames together with the closest D_3 filtergram times are given in Table II.C.2. There should be no large error due to different exposure times.

Fred Rosenberg at NRL has supplied us with tapes containing digitized output of microdensitometer scans of S082A data. Plates 20, 24 - 28, 32, 33 and 35 were scanned for the HeII 304, 256 and 243Å images. The H & D curve was provided for the 304Å line and it was used also for the 256 and 243Å lines. Some of these plates were considered for their 256 and 243Å intensities even though the 304Å results are solarized. Most of the scans were made of a 2500 x 2500 micron region as shown by the dashed lines in Fig. II. A. 1. The slit size used was 10 μ x 10 μ. With a solar diameter of 18.5 mm. the 10 μ steps correspond to a 1.04" resolution.

We have unpacked the tapes sent to us by NRL and have reconstructed the output and calculated intensities for 20 μ or 2.08" average slit size. 304Å total line intensities were obtained for plates 24, 25, 26, 32 and 34. 256Å and 243Å total line intensities were obtained from plates 24, 26, 28 and 32. Figs. II.C.1 - II.C.3 show the sun at 304Å from plates 24, 26 and 34. The flare is prominent at the eastern edge of AR 185 in all three photographs.

TABLE II.C.1

S082 Plates For 9 August 1973 Flare

Time UT	Plate No.	Wave Length	Exposure Time (sec)	Comments
15:20:32	2A022	ST	40	OK but exp is long for HeII. EPL in progress, possibly from small limb flare.
15:35	023	LG	160	Wrong roll and exp. too long
15:46:07	024	ST	9	Looks good. Exp. short enough so HeII is not solarized
15:30:20	025	ST	1 3/4	OK. exp. very short; flare kernel well-defined
15:54:00	026	ST	2¼	OK. exp. very short; flare kernel well-defined
15:54:05	027	ST	10	OK. flare kernel is solarized but still well-defined
15:54:17	028	ST	40	Exp. much too long for HeII-solarized
15:54:58	029	LG		He I 584 out of focus.
15:55:05	030			
15:55:27	031			
15:56:49	032	ST	2¼	Flare fogged by plate defect
15:56:53	033	ST	10	Flare slightly solarized
15:57:05	034	ST	½	Flare exposed OK
15:58:20	035	ST	40	Flare solarized

ST = Short Wavelength

LG = Long Wavelength

TABLE II.C.2

COINCIDENT FRAME TIMES
FLARE OF 9 AUGUST 1973

NRL Plate Number	Time	Exposure Time (sec)	Closest D_3 Filtergram Time
24	15:46:07	9	15:46:00
25	15:53:20	2	15:53:30
26	15:54:00	2¼	15:54:00
34	15:57:05	½	15:57:00

Plate 24 has an exposure time of 9 sec. and does not appear usually to be greatly solarized. Upon calculating the intensity at the 62500 points in the scanned area we find however, that 21608 are overexposed and do not fall on the established H & D curve. This means that only a lower limit to the 304Å intensity can be established over the entire flare area. Plates 25 and 26 have about 900 data points exceeding the limits of the H & D curve. All of these data points are overexposed. The overexposed area is about 15" x 30" with the long axis running N and S. This area corresponds very closely to the D_3 flare region. Fig. II.C.4 shows the relative intensity contours for NRL plate 26. The average background intensity is shown on the Fig. The intensities have been averaged over 10.4" x 10.4" areas. The area shown in the Fig. is 135" x 135". Intensities are shown in terms of the maximum intensity of 100. The larger 90 contour represents the D_3 flare region. Fig. II.C.5 shows this region on a scale expanded by 5 times. The entire D_3 flare region lies within the 100 contour region. The area inside the contour 100 is overexposed. Figs. II.C.6 and II.C.7 show the 256 and 243Å contour plots of the same region. The 256 and 243Å images are not solarized. We do not have definitive positions of the limb for these two wavelengths and thus can only postulate that the intense regions here correspond to the intense region in Fig. II.C.5.

The normal exposure times for S082Å were 160 sec., 40 sec., 10 sec. and 2.5 sec. Fortunately frame 34 was taken at the unusually short exposure time of .31 sec. Fig. II.C. 8 shows intensity contours for this frame. Even at this exposure time the flare center is solarized and we cannot obtain quantitative intensities within the relative intensity 100 contour.

S082B observations were taken of the 9 Aug. 73 flare in HeII. Fig. II.C.9 shows the flare in the H-α line of HeII at 1620Å. Unfortunately quantitative information was not available in time for this study.

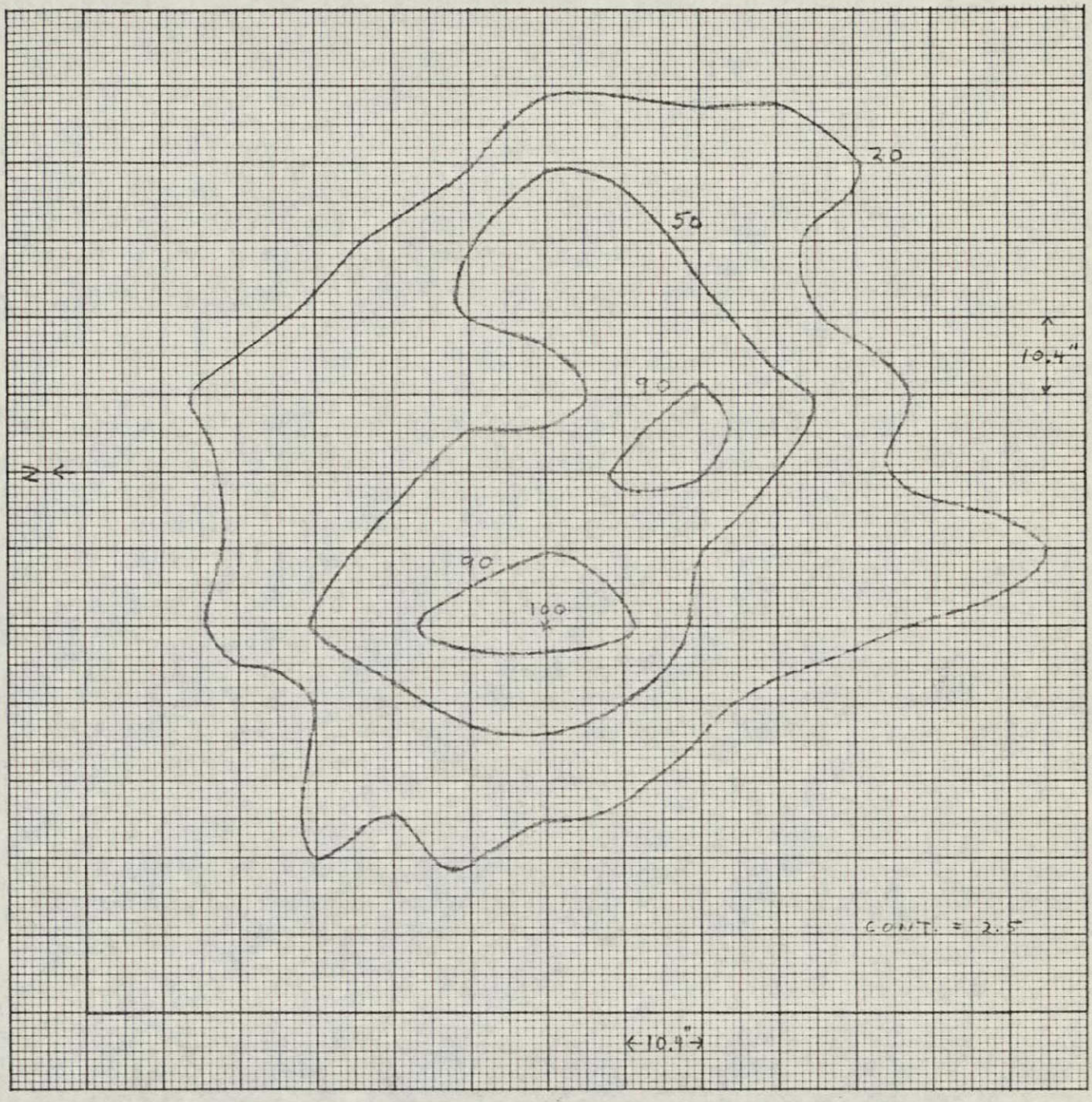

Figure II.C.4 304Å Line Intensities Relative to Maximum Intensity of 100.

UT 15:54:00
Area 2'15" x 2'15"

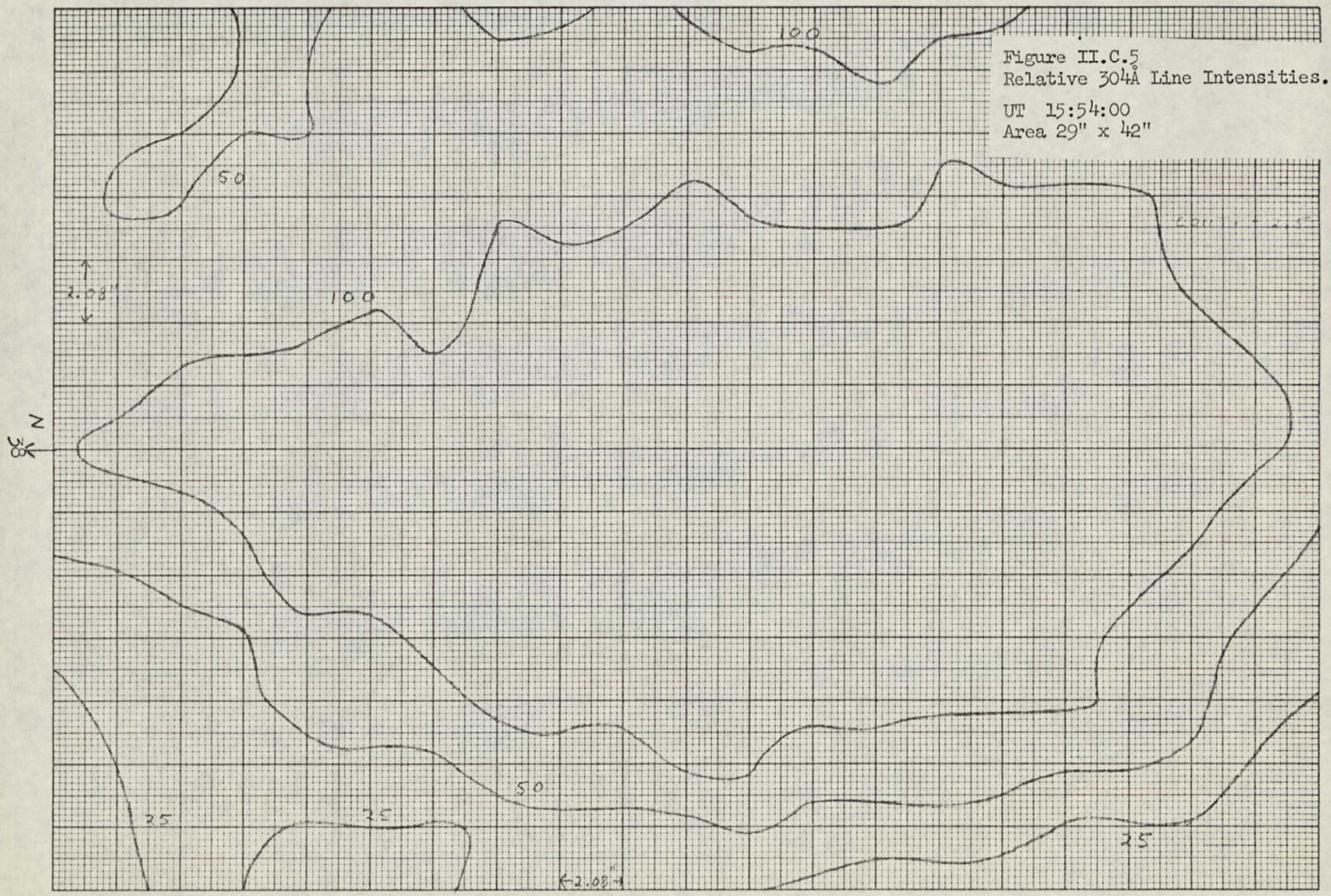

Figure II.C.5
Relative 304Å Line Intensities.

UT 15:54:00
Area 29" x 42"

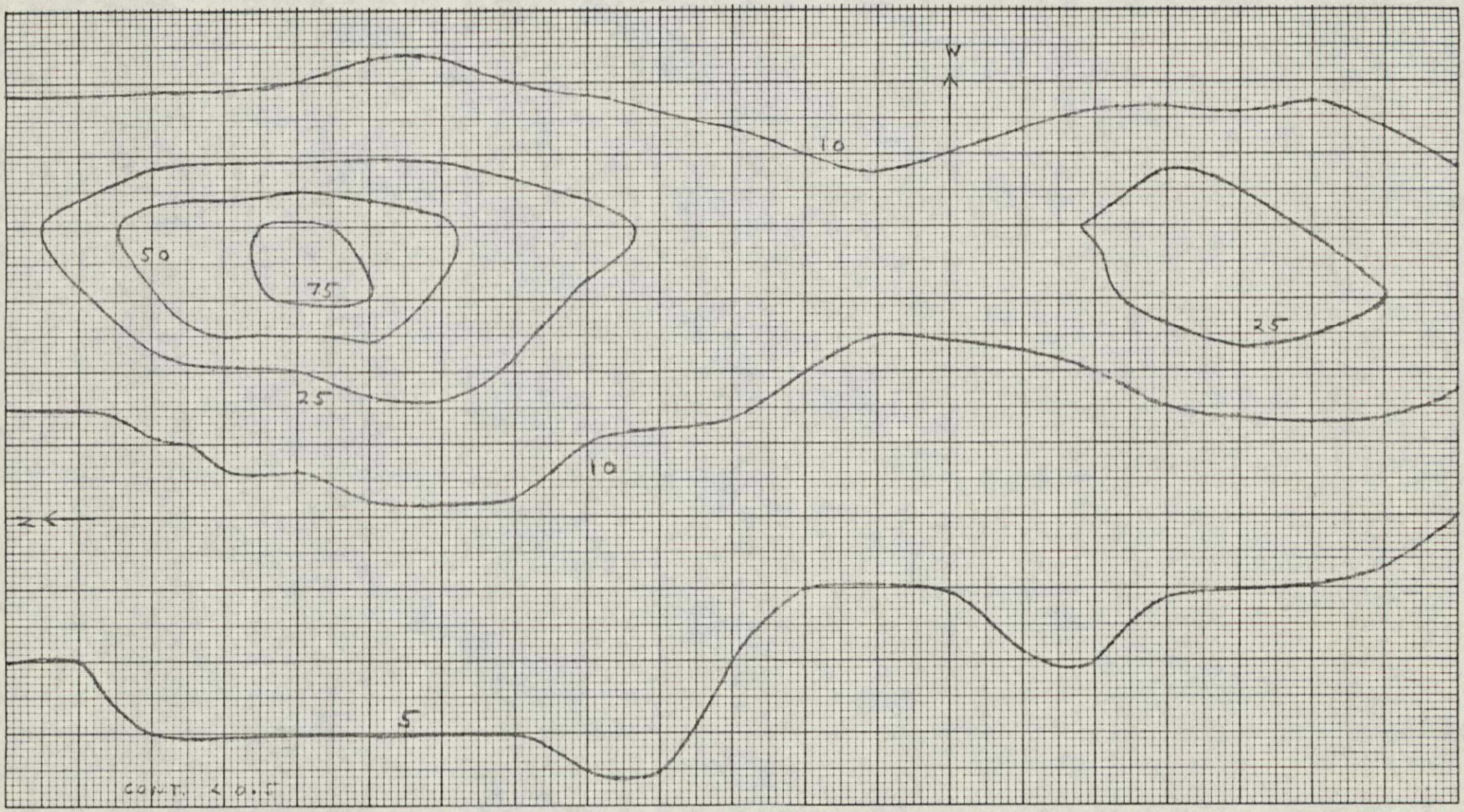

Figure II.C.6. Relative 256Å Line Intensities.

UT 15:54:00
Area 29" x 42"

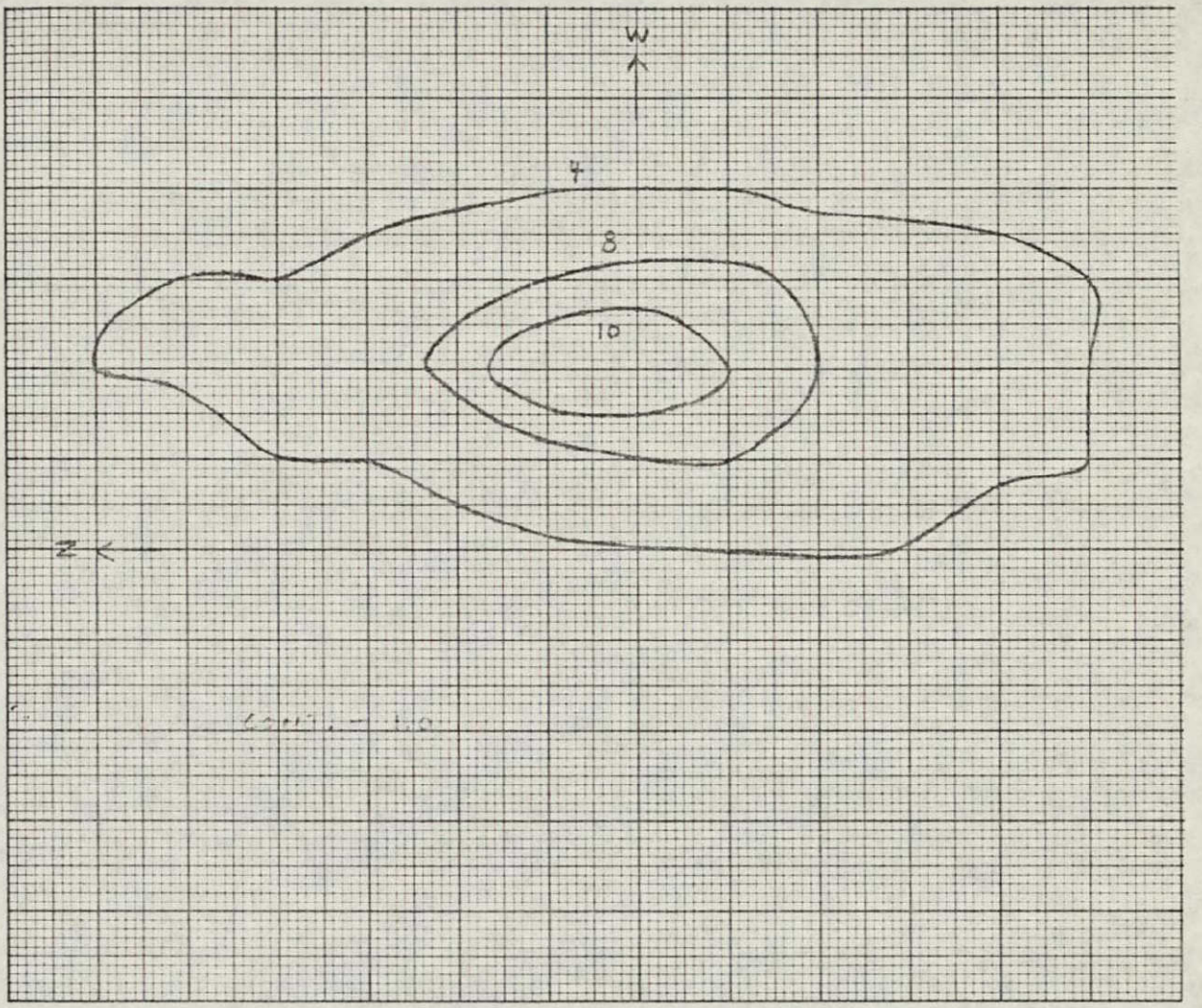

Figure II.C.7 Relative 243Å Line Intensities
UT 15:54:00
Area 29" x 42"

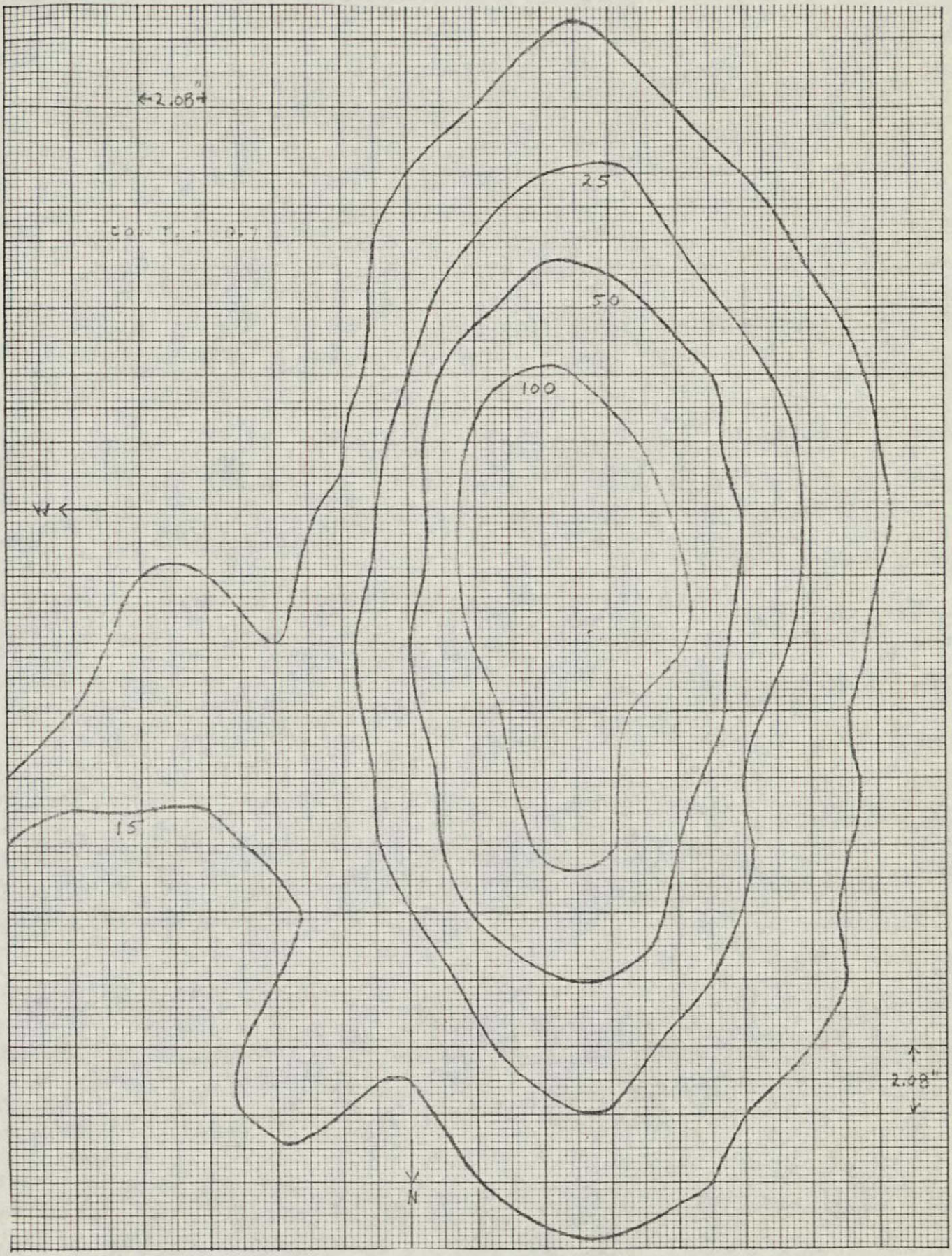

Figure II.C.8 Relative 304Å Line Intensities.
UT 15:57:05
Area 29" x 42"

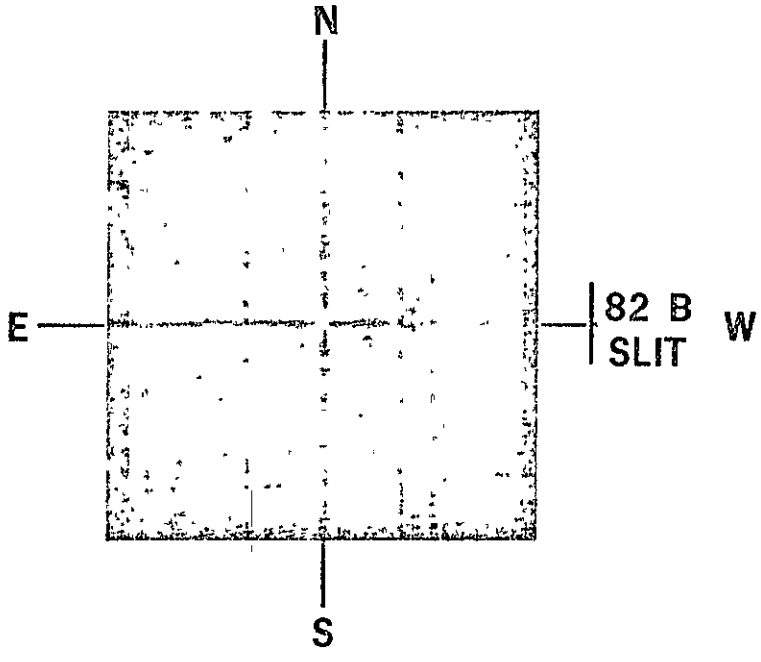

SO82 B POINTING
AUG 9, 1973 M2 FLARE
IN AR 185
Hα AT 15:54:00 UT

III. A Theoretical Model

The energy level model we use consists of 19 levels in HeI, 10 in He II and 1 in He III. All terms through n = 4 are included. The Tables in Appendix A show the energy levels and allowed lines in the model.

A plane-parallel slab irradiated on one side by a Planckian photospheric radiation field at radiation temperature T_r was chosen as the geometric model. The gas is assumed to be optically thin for all lines and continuua unless otherwise specified.

The rate equations for a statistically steady state have been set up as discussed in R1; Kulander, 1965; Kulander, 1976. The solution of the rate equations for the level populations is discussed in Appendix B. All radiative and collisional transitions between all terms were considered with the exception that excited levels only produce ground state ions upon ionization. These equations include an external Planckian radiation field at temperature T_r, and an adjustable parameter multiplying each line and continuum radiative intensity. The cross sections and reaction rates used have been discussed in R1 and Benson and Kulander, 1972. Solutions can be obtained parametrically for any arbitrary line and continuum radiation fields for specified election temperature and density.

The intensity in the given line from a plane-parallel layer is determined by the radiative transfer equation,

$$\mu \frac{dI_\nu}{d\tau_\nu} = I_\nu - S_\nu \qquad \text{III.A.1}$$

where $\cos^{-1}\mu$ represents the angle between the direction of propagation and the outward normal z, $\tau_\nu = \int k_\nu \, d_z$, S_ν is the source function, k_ν is the linear absorption coefficient and I_ν the specific intensity of the radiation. The source function on a microscopic basis can be written as

$$S_{u\ell} = \frac{2h\nu^3}{c^2} \frac{1}{[(g_u/g_\ell)(n_\ell/n_u)]-1}, \qquad \text{III.A.2}$$

where g represents the statistical weight. The populations n_u and n_ℓ are obtained from solution of the statistically steady state rate equation which for state i is

$$\sum_{j=i} (n_j P_{ji} - n_i P_{ij}) = \sum_j n_j P_{ji} = 0 \qquad \text{III.A.3}$$

$$P_{ii} = - \sum_{j \neq i} P_{ij}$$

where P_{ij} is the total transition rate from i to j per second per particle in the i state.

As shown in appendix B the line source function may be written

$$\frac{S_{u\ell}}{B_e} = \frac{\int_{u\ell} (J_\nu/B) \Phi_\nu \, d_\nu + \epsilon + i^*}{1 + \epsilon + \eta - \delta i} \qquad \text{III.A.4}$$

where J_ν is the mean intensity, B_e is the Planck function at T_e, Φ_ν is the normalized line profile $i^* = i/B$ and ϵ, η and i^* are non-LTE parameters obtained from the rate equation matrix. ϵ, η and i are specified in Appendix B.

III.B.1 Non-Equilibrium Parameters and Optical Depths

To obtain estimates of the line intensities we first need to know the non-equilibrium parameters ϵ , η , and i^* that enter the source function. ϵ is simply the ratio of collisional to radiative de-excitation of the upper line level. η and i^* must be obtained from the full rate equation matrix. We have obtained these values for the 584, 304 Å and D_3 lines for electron temperatures 10^4 through 5×10^4 ° K and electron densities 10^{10} through 10^{14} cm^{-3}. Tables III.B.1 through III.B.5 illustrate ϵ , η , and i^* for selected n_e and T_e values for the cases T, 1, 3 and 8 to be discussed shortly. (The number following each entry is the power of 10 by which the entry is multiplied.)

For the D_3 line i^*/η is shown in Fig. III.B.1 along with the theoretical limiting value

$$i^*/\eta = 1 - e^{-h\nu/kT}$$

which obtains in LTE .

The values given here are constant with depth since the various rates entering the rate equation matrix have been assumed constant. This is not in general true even for a layer of constant electron temperature since the various radiation fields are functions of position. We may obtain an indication of the effects of these varying radiation intensities by solving for the non-equilibrium parameters with different assumed radiation fields. Basically these radiation fields are functions of optical thickness becoming dominated by the external radiation when thin and approaching equilibrium values when completely thick.

In RI we made a parametric study of the effect of optical thickness in the resonance lines and continua upon the level populations. Level populations were obtained for various physically meaningful combinations of resonance lines and continua being optically thick or thin. Each resonance line was thus assumed to

TABLE III.B.1

CHARACTERISTIC VALUES OF ϵ, η, i^*

T_e(°K)	n_e (cm^{-3})	ϵ	η	i^*	Line (Å)	Case #
10^4	10^{10}	4.1-9	2.3-4	2.9-18	584	T
		"	"	5.1-14	"	3
		1.2-8	1.2-8	1.8-28	304	T
		"	"	"	"	3
	10^{11}	4.0-8	2.7-4	9.4-7	584	T
		"	"	"	"	1
		"	"	9.5-3	"	8
		2.304	6.1-2	5.8-3	5876	T
		"	5.0-2	8.8-3	"	1
		"	5.3-2	7.8-3	"	8
		1.2-7	5.8-8	4.8-8	304	T
		"	"	4.8-8	"	1
		"	"	5.2-2	"	8
	10^{13}	4.0-6	1.5-3	9.6-5	584	T
		"	"	"	"	1
		"	"	1.8-2	"	8
		2.3-4	1.02	5.7-2	5876	T
		"	.84	.10	"	1
		"	.49	.18	"	8
		1.2-5	4.8-6	4.7-6	304	T
		"	"	"	"	1
		"	"	4.7-2	"	8
	10^{14}	4.0-5	8.0-3	4.0-14	584	T
		"	"	8.3-13	"	3
		1.2-4	4.8-5	1.8-24	304	T
		"	"	"	"	3

TABLE III.B.2

CHARACTERISTIC VALUES OF ϵ, η, i^*

T_e(°K)	n_e (cm^{-3})	ϵ	η	i^*	Line (Å)	Case #
2×10^4	10^{10}	1.1-8	2.3-4	6.1-13	584	T
		"	"	3.8-3	"	3
		8.2-9	1.2-8	2.5-18	304	T
		"	"	"	"	3
	10^{11}	1.1-7	2.6-4	8.3-7	584	T
		"	"	"	"	1
		"	"	1.7-2	"	8
		2.8-4	5.4-2	3.4-3	5876	T
		"	6.0-2	2.8-3	"	1
		"	6.9-2	1.9-3	"	8
		8.2-8	5.5-8	3.4-8	304	T
		"	"	"	"	1
		"	"	6.3-4	"	8
	10^{13}	1.1-5	2.8-3	7.1-5	584	T
		"	"	"	"	1
		"	"	4.2-2	"	8
		2.8-2	1.19	4.2-2	5876	T
		"	.92	5.9-2	"	1
		"	.55	8.1-2	"	8
		8.2-6	5.7-6	3.4-6	304	T
		"	"	1.2-5	"	1
		"	"	1.5-3	"	8
	10^{14}	1.1-4	2.2-2	6.4-9	584	T
		"	"	4.9-7	"	3
		8.2-5	5.8-5	2.5-14	304	T
		"	"	"	"	3

TABLE III.B.3

CHARACTERISTIC VALUES OF ϵ, η, i^*

T_e(°K)	n_e (cm^{-3})	ϵ	η	i^*	Line (Å)	Case #
3×10^4	10^{10}	1.9-8	2.3-4	4.3-11	584	T
		"	"	"	"	3
		6.7-9	1.4-8	6.1-15	304	T
		"	"	4.2-9	"	3
	10^{11}		(1.304)	(9.8-7)		
		1.9-7	2.7-4	9.2-7	584	T
		"	"	"	"	1
		"	"	(4.2-2) 4.0-2	"	8
		3.0-4	(6.5-2) 7.5-2	(1.5-3) 1.5-3	5876	T
		"	"	"	"	1
		"	(5.7-2) 6.6-2	(2.2-3) 2.1-3	"	8
		6.7-8	(7.0-8) 7.9-8	3.0-8	304	T
		"	"	"	"	1
		"	"	3.0-3	"	8
	10^{13}		(3.7-3)	(2.2-5)		
		1.9-5	4.1-3	7.3-5	584	T
		"	"	"	"	1
		"		(6.9-2)		
		"	"	6.8-2	"	8
		3.0-2	(.88) 1.30	3.6-2	5876	T
		"	"	"	"	1
		"	(.68) :68	(5.6-2) 5.7-2	"	8
		6.7-6	(1.1-5) 1.1-5	3.0-6	304	T
		"	"	"	"	1
		"	"	7.0-3	"	8
	10^{14}	6.7-5	1.2-4	5.8-11	584	T
		"	"	1.4-8	"	3
		1.9-4	3.4-2	4.0-7	304	T
		"	"	"	"	3

TABLE III.B5

CHARACTERISTIC VALUES OF ϵ, η, i^*

T_e(°K)	n_e (cm^{-3})	ϵ	η	i^*	Line (Å)	Case #
5×10^4	10^{10}	3.8-8	2.3-4	1.6-9	584	T
		"	2.0-4	9.0-10	"	3
		5.2-9	1.9-8	3.4-12	304	T
		"	"	8.1-6	"	3
	10^{11}	3.8-7	2.8-4	1.2-6	584	T
		"	2.3-4	9.2-7	"	1
		"	"	3.6-2	"	8
		3.4-4	8.1-2	1.2-3	5876	T
		"	6.4-2	1.1-3	"	1
		"	4.0-2	"	"	8
		5.2-8	1.5-7	3.0-8	304	T
		"	"	"	"	1
		"	"	1.2-2	"	8
	10^{13}	3.8-5	6.1-3	8.6-3	584	T
		"	5.9-3	"	"	1
		"	6.3-3	.12	"	8
		3.4-2	1.43	2.8-2	5876	T
		"	1.40	"	"	1
		"	.91	4.0-2	"	8
		5.2-6	2.6-5	2.7-6	304	T
		"	"	"	"	1
		"	"	2.5-2	"	8
	10^{14}	3.8-4	2.7-4	3.0-8	304	T
		"	5.8-2	"	"	3
		5.2-5	2.7-4	3.0-8	304	T
		"	"	2.7-5	"	3

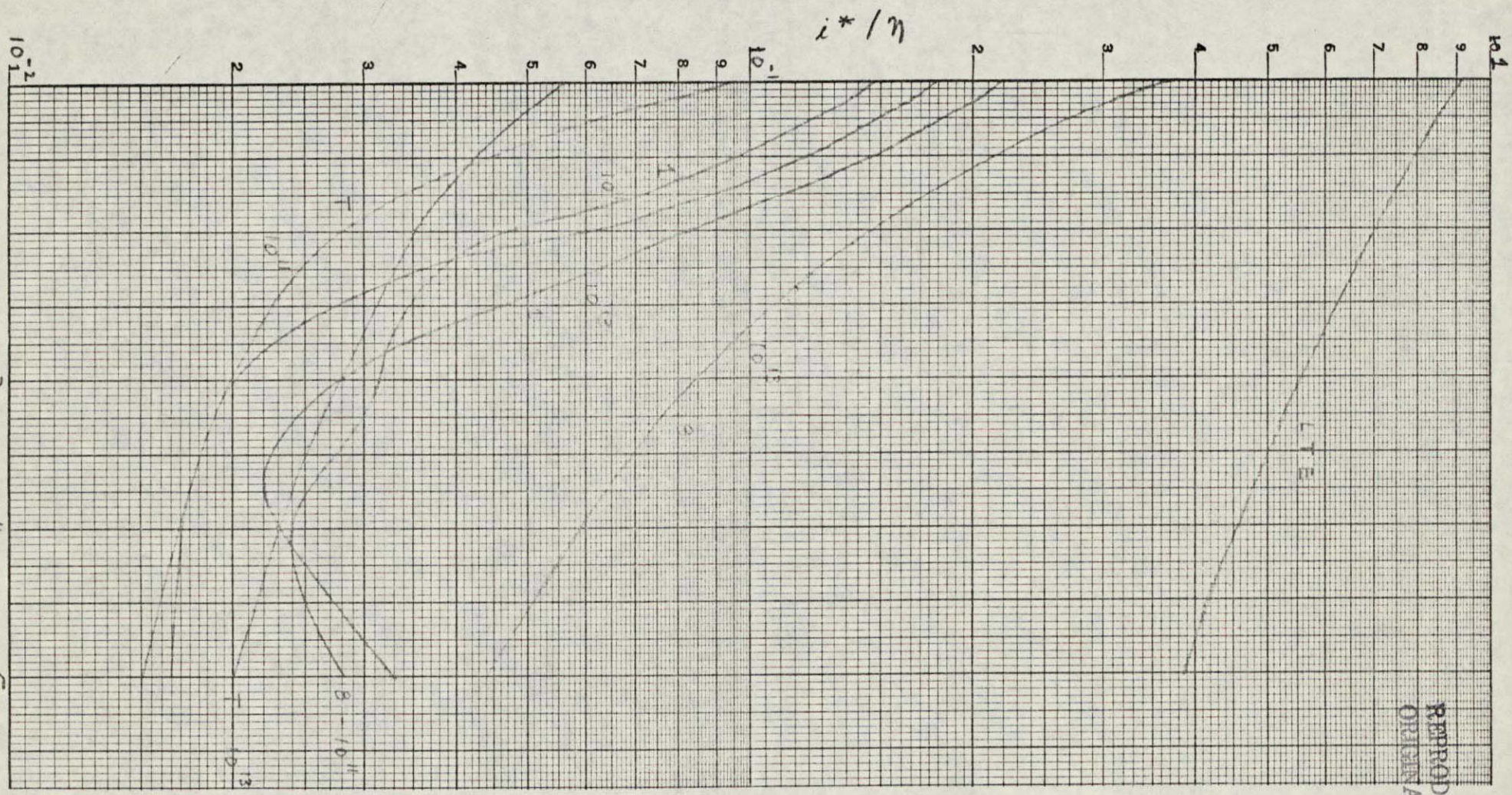

Figure III.B.1 Ratio of i^* to η for D_γ Line. Curves are labeled with the case number and n_e value.

have a net radiative bracket (NRB) of either 0 (completely thick) or 1 (thin). For each specified electron temperature, calculations were made for combinations of net radiative brackets corresponding to layers of varying total thickness. There are three resonance lines in the model for both HeI and HeII. These six lines together with the Lyman continua for each ion are allowed to become optically thick in our calculation. Thus, there are eight lines and continua which can be optically thick or thin depending upon the physical thickness of the layer.

Nine solutions for the level populations were made for each T_e and n_e. These refer to a solution where all lines and continua were optically thin (labeled T) and eight other solutions labeled 1-8 which correspond to the combinations of optical thick lines and continua given in Table III.B.6. In this Table (1), (2) and (3) refer to the 584, 537 and 522 Å lines of HeI respectively, and (4) refers to the Lyman continuum of HeI. Similarly the numbers (5-8) refer to the 304, 256, 243 Å lines and the Lyman continuum of HeII respectively. When a number appears in Table III.B.6 the corresponding transition has been assumed optically thick (i.e., in radiative detailed balance) in obtaining rate coefficients for the level population solutions. Transitions not appearing in the Table are assumed optically thin. It is noted that progressing from Case 1 to 8 corresponds in general to the layer becoming thicker. Case 8 always corresponds to all eight lines and continua becoming optically thick. For example, with $T_e = 30{,}000°$ K Case 4 represents the NRB = 0 in the first three resonance lines of HeI and the first resonance line of HeII.

In RI we also determined the optical depths in a number of lines of a 1000 km thick layer. Since these results are very pertinent here we shall reproduce them again. For each of the same cases given in Table III.B.6 we have obtained the line center optical thickness in the 584, 304, 10830 Å, D_3 lines and at the threshold of the Lyman continua of HeI and II.

Table III.B.6

OPTICALLY THICK LINES CHOSEN

Case Number

Temperature	1	2	3	4	5	6	7	8
10^4	1	1,2	1-3	1-4	1-5	1-6	1-7	1-8
$2x10^4$	1	1,2	1-3	1-3 5	1-3 5,6	1-3 5-7	1-3 5-8	1-8
$3x10^4$	5	5,6	5-7	1 5-7	1,2 5-7	1-3 5-7	1-3 5-8	1-8
$4x10^4$	5	5,6	5-7	5-8	1 5-8	1,2 5-8	1-3 5-8	1-8
$5x10^4$	5	5,6	5-7	5-8	1 5-8	1,2 5-8	1-3 5-8	1-8

The optical thicknesses are given in Tables III.B.7 through III.B.11. The number following each entry is the power of 10 by which the entry is multiplied. We note that the 10830 and D_3 lines can become thick for high electron densities even at 50,000° K. These lines do not become thick at 10,000° K. There are many cases in which a number of lines and continua are optically thick. This does not mean, however, that simultaneous transport equations must be solved for these lines and continua. Which line and continuum radiation fields must be obtained simultaneously depends upon the level population being sought as well as the temperature, density, and layer optical thickness.

Table III.B.7

OPTICAL THICKNESS - 1000 KM LAYER

T_e = 10,000 °K

TRANSITION	n_e	Case T	1	2	3	4	5	6	7	8
	10^{10}									
584		3.7+4*	=	=	=	1.3+4	=	=	=	=
504		7.6	=	=	=	4.1	=	=	=	=
5876		2.8-8	1.1-5	2.1-5	2.7-5	8.0-4	=	=	=	=
10830		2.6-7	1.0-4	1.9-4	2.5-4	7.4-3	=	=	=	=
304		1.5-2	9.6			8.6+2	=	=	=	=
228		1.4-6	9.3-4	1.8-3	2.4-3	8.3-2	=	=	=	=
	10^{11}									
584		3.7+5	=	=	=	=	=	=	=	=
504		76	=	=	=	=	=	=	=	=
5876		1.3-6	1.7-4	2.2-4	3.7-4	6.7-3	=	=	=	=
10830		1.2-5	1.2-3	2.1-3	3.4-3	6.2-2	=	=	=	=
304		.046				1.6+3	=	=	=	=
228		4.4-6	1.0-3	1.9-3	3.1-3	.15	=	=	=	=
	10^{12}									
584		3.7+6	=	=	=	=	=	=	=	=
504		7.6+2	=	=	=	=	=	=	=	=
5876		1.5-5	1.1-3	2.4-3	4.7-3	1.5-2	=	=	=	=
10830		1.2-4	8.6-3	2.0-2	3.7-2	0.12	=	=	=	=
304		0.10				1.3+3	=	=	=	=
228		9.3-6	1.0-3	2.8-3	6.0-3	1.2-1	=	=	=	=
	10^{13}									
584		3.7+7	=	=	=	=	=	=	=	=
504		7.6+3	=	=	=	=	=	=	=	=
5876		2.1-4	1.0-2	3.1-2	4.1-2	6.2-2	=	=	=	=
10830		1.4-3	4.7-2	0.13	0.17	0.26	=	=	=	=
304		0.56		1.3+22	2.5+2	1.1+3	=	=	=	=
228		5.4-5	2.7-3	1.3-2	2.4-2	1.0-1	=	=	=	=
	10^{14}									
584		3.7+8	=	=	=	=	=	=	=	=
504		7.6+4	=	=	=	=	=	=	=	=
5876		5.6-3	0.15	0.24	0.26	0.29	=	=	=	=
10830		1.4-2	0.37	0.54	0.59	0.66	=	=	=	=
304		4.7	1.7+2	5.0+2	6.1+2	9.3+2	=	=	=	=
228		4.5-4	1.6-2	4.8-2	5.9-2	9.0-2	=	=	=	=

* The number following each entry is the power of 10 by which the entry is multiplied.

Table III.B.8

OPTICAL THICKNESS - 1000 KM LAYER

$T_e = 2 \times 10^4$ °K

TRANSITION	n_e	Case T	1	2	3	4	5	6	7	8
	10^{10}									
584		1.7+3	3.4	0.92	0.52	=	=	=	7.0-3	=
504		0.36	7.2-4	1.9-4	1.1-4	=	=	=	1.5-6	=
5876		1.7-3	1.8-3	1.7-3	=	=	=	=	9.6-4	=
10830		1.6-2	1.7-2	1.6-2	=	=	=	=	9.3-3	=
304		1.5+3	2.8+3	=	=	=	=	=	2.0+3	=
228		0.10	0.19	=	=	=	=	=	0.13	=
	10^{11}									
584		2.0+4	2.2+2	61.	26.	=	=	=	1.0	=
504		5.7	6.3-2	1.7-2	7.4-3	=	=	=	2.9-4	=
5876		4.3-2	0.11	=	=	=	=	=	3.3-2	=
10830		0.38	1.0	0.86	0.93	=	=	=	2.9-4	=
304		5.1+3	2.1+4	=	=	=	=	=	=	=
228		0.43	1.8	=	=	=	=	=	=	=
	10^{12}									
584		2.3+5	1.0+4	2.0+3	5.6+2	=	=	=	100.	=
504		65.	2.8	0.56	0.16	=	=	=	2.8-2	=
5876		0.90	4.3	4.0	3.1	=	=	=	1.0	=
10830		5.3	24.	22.	17.	=	=	=	=	=
304		3.3+4	2.0+5	=	=	=	=	=	=	=
228		2.7	16.	=	=	=	=	=	=	=
	10^{13}									
584		2.0+6	1.2+5	1.7+4	8.5+3	=	=	=	5.2+3	=
504		6.1+2	37.	5.2	2.6	=	=	=	1.6	=
5876		18.	63.	48.	38.	=	=	=	28.	=
10830		37.	1.3+2	90.	69.	=	=	=	52.	=
304		4.0+5	1.9+6	=	=	=	=	=	=	=
228		36.	170.	=	=	=	=	=	=	=
	10^{14}									
584		2.0+7	1.2+6	3.8+5	3.0+5	=	=	=	2.6+5	=
504		5.8+3	350.	110.	87.	=	=	=	75.	=
5876		2.8+2	7.7+2	5.4+2	5.1+2	=	=	=	4.8+2	=
10830		3.3+2	8.8+2	5.8+2	5.4+2	=	=	=	5.1+2	=
304		5.1+6	1.9+7	=	=	=	=	=	=	=
228		450.	1.7+3	=	=	=	=	=	=	=

56

Table III.B.9

OPTICAL THICKNESS - 1000 KM LAYER

$T_e = 3 \times 10^4$ °K

TRANSITION	n_e	Case T	1	2	3	4	5	6	7	8
	10^{10}									
584		23.	=	22.	21.	2.5-2	5.2-3	2.7-3	1.7-5	1.6-5
504		8.4-3	=	=	8.2-3	1.0-6	2.0-7	1.0-7	5.9-6	6.0-11
5876		1.3-3	=	=	1.2-3	7.7-4	7.0-4	=	4.3-6	3.2-6
10830		1.2-2	=	=	1.1-2	7.2-3	6.5-3	6.4-3	4.0-5	3.0-5
304		1.6+3	=	=	=	=	=	=	10.	=
228		0.18	=	=	0.17	=	=	=	1.1-3	=
	10^{11}									
584		6.3+2	=	=	=	2.0	0.43	0.15	8.8-3	2.6-4
504		0.19	=	=	=	7.2-4	1.5-4	5.0-5	3.2-6	1.0-7
5876		6.8-2	=	=	=	5.2-2	4.5-2	=	2.9-3	8.2-5
10830		0.57	=	=	=	0.43	0.37	=	2.4-2	7.0-5
304		1.6+4	=	=	=	=	=	=	1.0+3	=
228		1.7	=	=	=	=	=	=	0.10	=
	10^{12}									
584		7.3+3	=	=	=	62.	9.6	2.5	1.0	0.13
504		2.6	=	=	=	.22	3.4-3	8.9-4	3.6-4	4.6-5
5876		1.5	=	=	=	1.4	=	1.1	0.42	0.15
10830		6.8	=	=	=	6.2	5.9	4.7	1.8	0.63
304		1.6+5	=	=	=	=	=	=	6.4+4	=
228		18.	=	=	=	=	=	=	7.0	=
	10^{13}									
584		4.8+4	=	=	=	6.5+2	76.	38.	32.	17.
504		17.	=	=	=	0.23	2.7-2	1.4-2	1.2-2	6.4-3
5876		22.	=	=	=	18.	15.	12.	10.	7.3
10830		32.	=	=	=	25.	19.	15.	13.	10.
304		1.6+6	=	=	=	=	=	=	1.4+6	=
228		1.8+2	=	=	=	=	=	=	1.5+2	=
	10^{14}									
584		3.1+5	3.3+5	3.7+5	=	5.9+3	1.8+3	1.4+3	=	1.1+3
504		1.2+2	=	1.3+2	=	2.3	0.69	0.48	=	0.38
5876		2.0+2	=	2.4+2	=	1.9+2	1.4+2	1.3+2	=	1.2+2
10830		2.6+2	=	2.1+2	=	1.7+2	1.2+2	1.1+2	=	1.0+2
304		1.5+7	=	=	=	1.6+7	=	=	=	=
228		1.8+3	=	=	=	=	=	=	=	=

Table III.B.10

OPTICAL THICKNESS - 1000 KM LAYER

$T_e = 4 \times 10^4$ °K

TRANSITION	n_e	Case T	1	2	3	4	5	6	7	8
	10^{10}									
584		1.9	=	1.5	0.37	1.9-4	1.0-7	1.7-8	8.5-9	5.5-11
504		7.6-4	=	4.5-4	1.5-4	7.6-8	4.0-11	6.8-12	3.4-12	2.2-14
5876		8.3-4	=	6.4-4	1.6-4	1.6-8	1.4-8	1.2-8	=	6.6-9
10830		7.7-3	=	5.9-3	1.5-3	7.7-7	1.3-7	1.0-7	=	6.0-8
304		1.5+3	=	1.2+3	2.9+2	2.9-2	=	=	=	=
228		0.18	=	0.11	.035	3.5-6	=	=	=	=
	10^{11}									
584		40.	38.	33.	15.	6.7-3	4.3-5	8.0-6	2.7-7	4.7-9
504		1.7-2	=	1.5-2	7.0-3	2.8-6	1.8-8	3.4-9	1.1-10	2.0-12
5876		0.32	0.31	0.27	0.13	5.6-6	=	3.8-6	=	1.2-6
10830		0.26	0.25	0.21	0.11	4.5-5	=	3.9-5	=	1.3-5
304		1.4+4	=	1.3+4	7.6+3	2.8	=	=	=	=
228		1.8	=	1.6	0.81	3.6-4	=	=	=	=
	10^{12}									
584		4.2+2	4.1+2	3.7+2	2.5+2	0.82	8.1-3	1.1-3	2.5-4	3.3-5
504		0.17	=	0.15	0.11	3.4-4	3.4-6	4.7-7	1.2-7	1.4-8
5876		0.69	0.67	0.61	0.41	1.4-3	=	=	1.1-3	4.0-4
10830		2.6	2.5	2.3	1.5	5.0-3	=	4.9-3	4.0-3	1.4-3
304		1.5+5	1.4+5	1.3+5	8.7+4	2.9+2	=	=	=	=
228		18.	17.	16.	11.	3.6-2	=	=	=	=
	10^{13}									
584		2.7+3	2.5+3	2.3+3	1.6+3		0.80	0.10	4.5-2	2.0-2
504		1.0	0.92	0.84	0.68	2.2-2	2.1-4	3.6-5	1.8-5	7.7-6
5876		9.1	8.7	8.0	5.6	0.19	0.16	0.13	0.10	8.0-2
10830		11.	10.	9.2	6.5	0.22	0.19	0.14	0.12	8.5-2
304		1.5+6	1.4+6	1.2+6	8.8+5	3.0+4	=	=	=	=
228		180.	170.	160.	100.	3.6	=	=	=	=
	10^{14}									
584		2.1+4	2.0+4	1.7+4	1.2+4	3.1+3				9.0
504		8.4	7.8	6.4	3.0	0.77	1.3-2	4.0-3	3.2-3	2.2-3
5876		99.	95.	83.	58.	15.	12.	10.	9.0	8.3
10830		76.	72.	62.	45.	11.	10.	7.0	6.6	6.0
304		1.4+7	=	1.2+7	9.0+6	2.3+6	=	=	=	=
228		1.8+3	1.7+3	1.4+3	1.2+3	3.0+2	=	=	=	=

Table III.B.11

OPTICAL THICKNESS - 1000 KM LAYER

$T_e = 5 \times 10^4$ °K

TRANSITION	n_e	Case T	1	2	3	4	5	6	7	8
	10^{10}									
584		0.35	0.21	4.2-2	3.5-3	2.1-7	-	-	-	-
504		1.5-4	9.0-5	1.8-5	1.5-6	9.0-11	-	-	-	-
5876		5.4-4	3.4-4	6.5-5	5.3-6	3.2-10	-	-	-	-
10830		4.9-3	3.0-3	6.0-4	5.0-5	3.0-9	-	-	-	-
304		1.3+3	7.8+2	1.6+2	13.	7.8-4	=	=	=	=
228		0.18	0.11	2.2-2	1.8-3	1.1-7	=	=	=	=
	10^{11}									
584		6.6	4.0	1.3	0.26	4.0-5	-	-	-	-
504		3.0-3	1.8-3	5.9-4	1.2-4	1.8-8	-	-	-	-
5876		1.8-2	1.1-2	3.6-3	7.2-4	1.1-7	-	-	-	-
10830		0.14	8.4-2	2.8-2	5.6-3	8.4-7	-	-	-	-
304		1.3+4	7.8+3	2.6+3	5.2+2	7.8-2	=	=	=	=
228		1.8	1.1	0.36	7.2-2	1.1-5	=	=	=	=
	10^{12}									
584		62.	37.	12.	3.1	3.7-3	-	-	-	-
504		3.0-2	1.8-2	5.8-3	1.5-3	1.8-6	-	-	-	-
5876		0.37	0.22	7.4-2	1.8-2	2.2-5	-	-	-	-
10830		1.2	0.75	0.24	6.0-2	7.2-5	-	-	-	-
304		1.3+5	7.8+4	2.6+4	6.5+3	7.8	=	=	=	=
228		18.	11.	3.6	0.90	1.1-3	=	=	=	=
	10^{13}									
584		4.1+2	2.4+2	82.	20.	0.25	4.0-3	4.5-4	2.3-4	9.0-5
504		0.18	0.11	3.6-2	8.8-3	1.1-4	1.8-6	2.0-7	1.0-7	4.0-8
5876		4.8	2.9	0.96	0.24	2.9-3	2.6-3	2.2-3	1.7-3	1.3-3
10830		4.9	2.9	1.0	0.25	2.9-3	2.6-3	2.1-3	1.7-3	1.3-3
304		1.3+6	7.8+5	2.6+5	6.5+4	7.8+2	=	=	=	=
228		180.	110.	36.	8.8	0.11	=	=	=	=
	10^{14}									
584		3.0+3	1.9+3	5.0+2	160.	19.	0.35	0.11	8.5-2	5.9-2
504		1.4	0.84	0.22	7.0-2	8.9-3	1.6-4	5.1-5	4.0-5	2.8-5
5876		47.	30.	7.8	2.4	0.29	0.25	0.20	=	=
10830		33.	21.	5.6	1.7	0.21	0.18	0.14	=	=
304		1.3+7	7.8+6	2.1+6	6.5+5	7.8+4	=	=	=	=
228		1.8+3	1.1+3	2.9+2	9.0+1	11.	=	=	=	=

III.B.2 D_3 Line Profiles and Transmitted Intensities

Using the line source function of Eq. III.A.4 for a finite plane-parallel layer above the photosphere we may obtain the emergent intensity $[I_\nu(0,\mu)/B_e] = I_\nu^*(0,\mu)$ from the surface of a layer of optical thickness t_1 at angle $\cos^{-1}\mu$ with respect to the normal, from

$$I_\nu^*(0,\mu) = \int_0^{t_1} \varphi_\nu S_\nu^* \exp(-\int_0^t \varphi_\nu \, dt/\mu) \, dt/\mu \quad . \qquad \text{III.B.1}$$

With φ_ν a constant with depth, the photospheric radiation being given by B_r and assuming no continuous absorption the emergent intensity becomes (see Appendix B for details)

$$I_\nu^*(0,\mu) = \bar{\omega}\,\varphi_\nu \sum_\alpha L_\alpha \left[\frac{1 - e^{-(k_\alpha + \varphi_\nu/\mu)t_1}}{\varphi_\nu + k_\alpha\mu} + \frac{e^{-k_\alpha t_1} - e^{-\varphi_\nu t_1/\mu}}{(\varphi_\nu - k_\alpha\mu)}\right]$$

$$+ \bar{\omega}\,\varphi_\nu \sum_\alpha F_\alpha \left[\frac{e^{-k_\alpha t_1} - e^{-\varphi_\nu t_1/\mu}}{\varphi_\nu - k_\alpha \mu}\right] + \Delta\left(1 - e^{-\varphi t_1/\mu}\right)$$

$$+ \frac{B_r}{B_e} e^{-\varphi_\nu t_1/\mu} \qquad \text{III.B.2}$$

This is a homogeneous slab solution assuming an Eddington approximation which we shall use in obtaining transmitted intensities.

D3 line profiles have been calculated for a wide range of values of ϵ, η, i^* and t_1 from Eq. III.B.2. Figure III.B.2 illustrates results for $T_r = 6000^\circ K$, $T_e = 20{,}000^\circ K$, $n_e = 10^{12}$ cm^{-3} for various values of ϵ, η, i^* and t_1.

The D_3 filter has a Gaussian profile with a total half width of 0.40 Å. The transmission of the filter can be written as

$$T_v = \text{Exp} - \left[\frac{\sqrt{\ln 2}}{0.20}\,\Delta\lambda_D\, v\right]^2 \qquad \text{III.B.3}$$

where $v = \Delta\lambda/\Delta\lambda_D$ and

$$\Delta\lambda_D = \frac{\lambda}{c}\sqrt{2k\,T_e/M}$$

Some characteristic values for $\Delta\lambda_D$ are given in Table III.B.1. The total integrated intensity observed through the filter is

$$\int T_\nu \, I_\nu \, d\nu \quad .$$

We define the total transmission TT of the filter as

$$TT = \frac{\int T_\nu \, I_\nu \, d\nu}{\int I_\nu \, d\nu}$$

Figure III.B.2 illustrates values of TT for the case $\epsilon = 10^{-3}$, $Te = 20{,}000^\circ K$, $\mu = 1$, for various values of η and i^*. The curves are labeled with the exponents of η and i^*, for example the curve $\eta = 10^{-3}$, $i^* = 10^{-4}$ is labeled 3,4.

The most useful quantity for our interpretation is the total transmitted line intensity with respect to the total transmitted continuum intensity, i.e.

$$R = \frac{\int T_\nu \, I_\nu \, d\nu}{I_o \int T_\nu \, d\nu} \quad .$$

Selected values for R are shown in Figures III.B.3 to III.B.6 for $T_r = 6000^\circ K$, $\mu = 1$, $Te = 2 \times 10^4$ and 4×10^4 and for ϵ values 10^{-1}, 10^{-2}, 10^{-3} and 10^{-4}. The curve for $\epsilon = 10^{-2}$, $\eta = 10^{-3}$, $i^* = 10^{-4}$ for example is labeled 2,3,4. I_o has been set equal to $B(T_r)$.

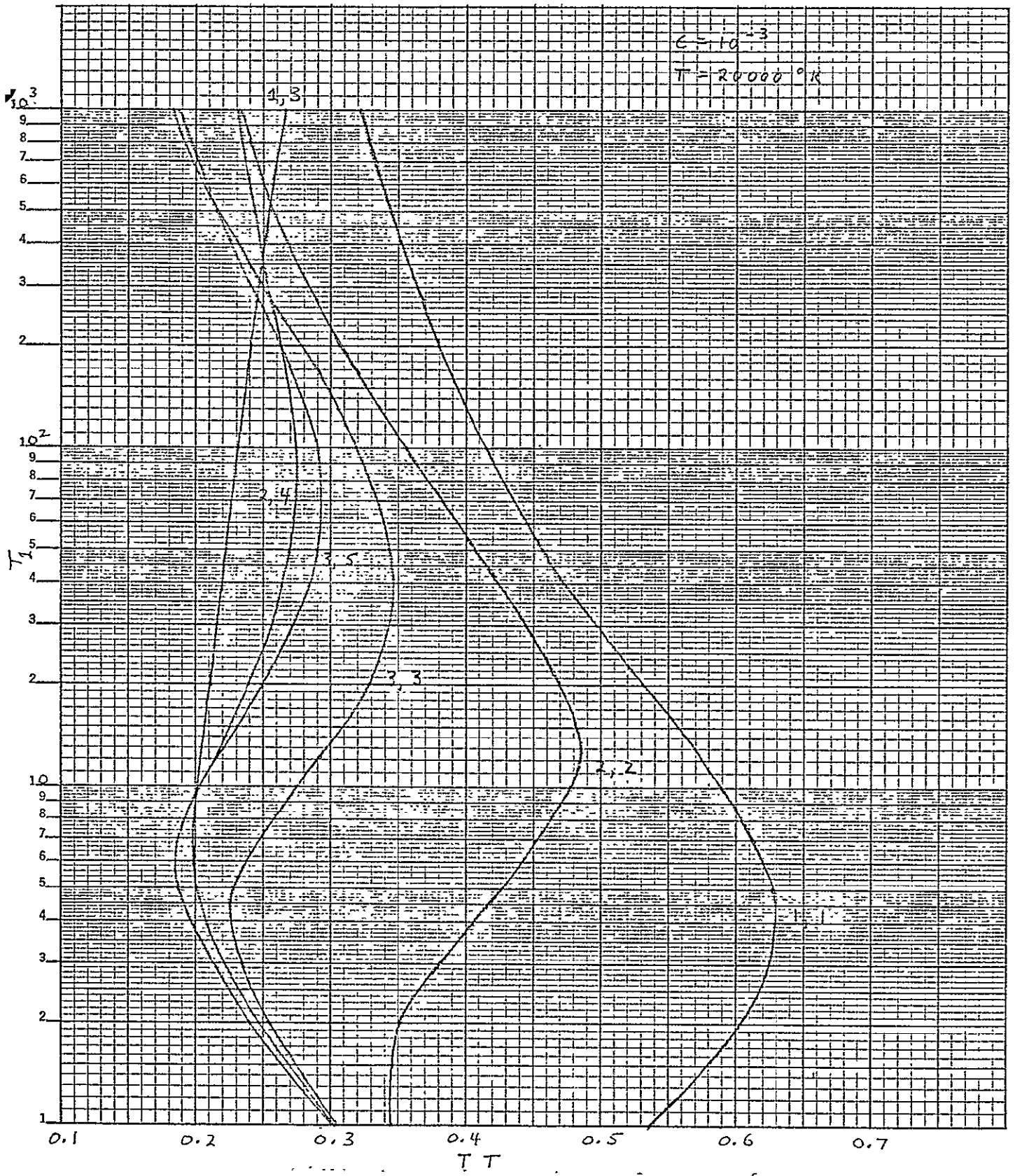

Figure III.B.3 Total Transmission for $T_e = 20{,}000^\circ K$, $\epsilon = 10^{-3}$, $\mu = 1$. Curves are labeled with negative exponent values of η and i^*.

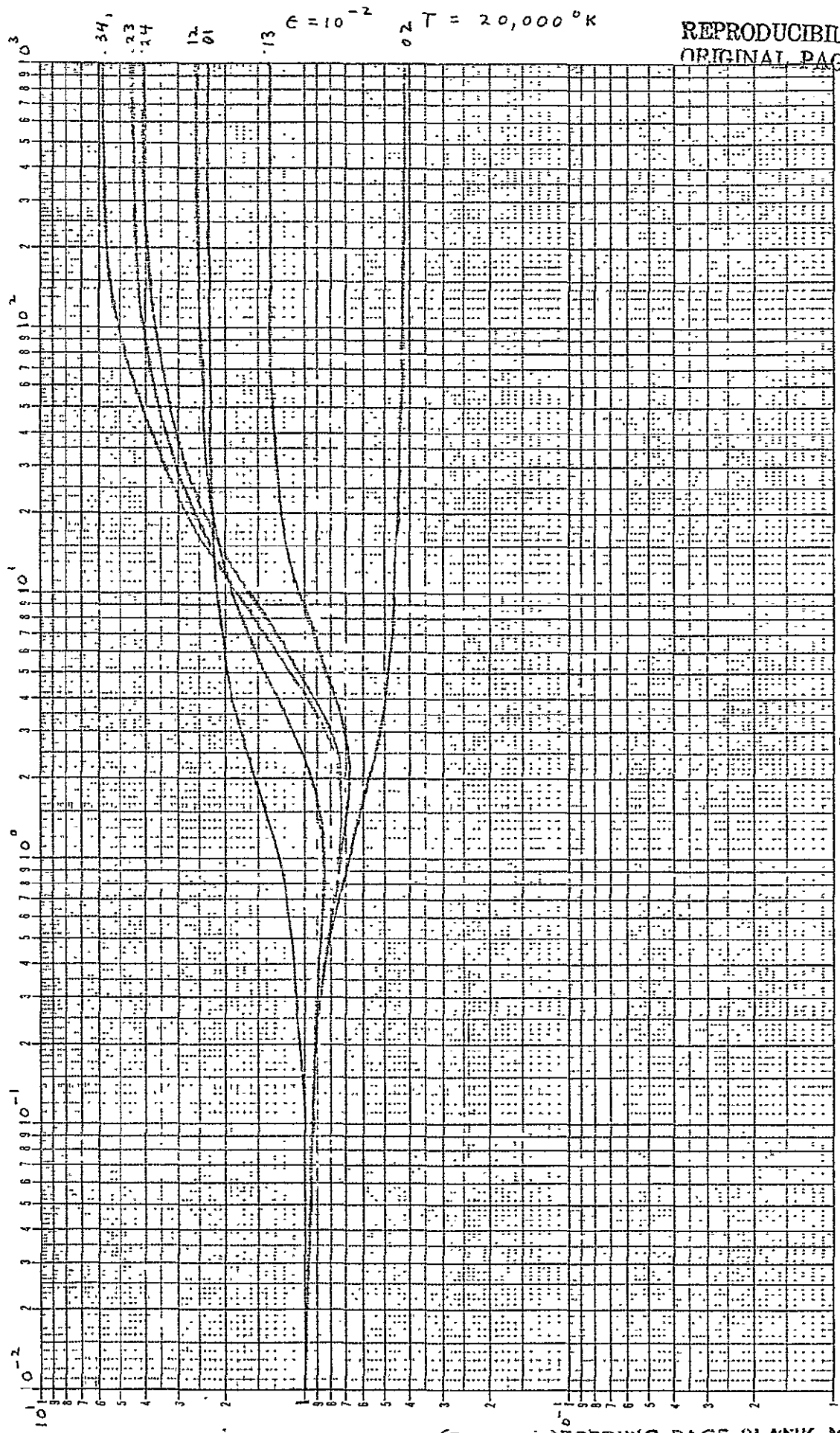

Figure III.B.5 Total Transmitted Line Intensity with Respect to Continuum for $\epsilon = 10^{-2}$. Curves are labeled with negative exponent values of η and i.

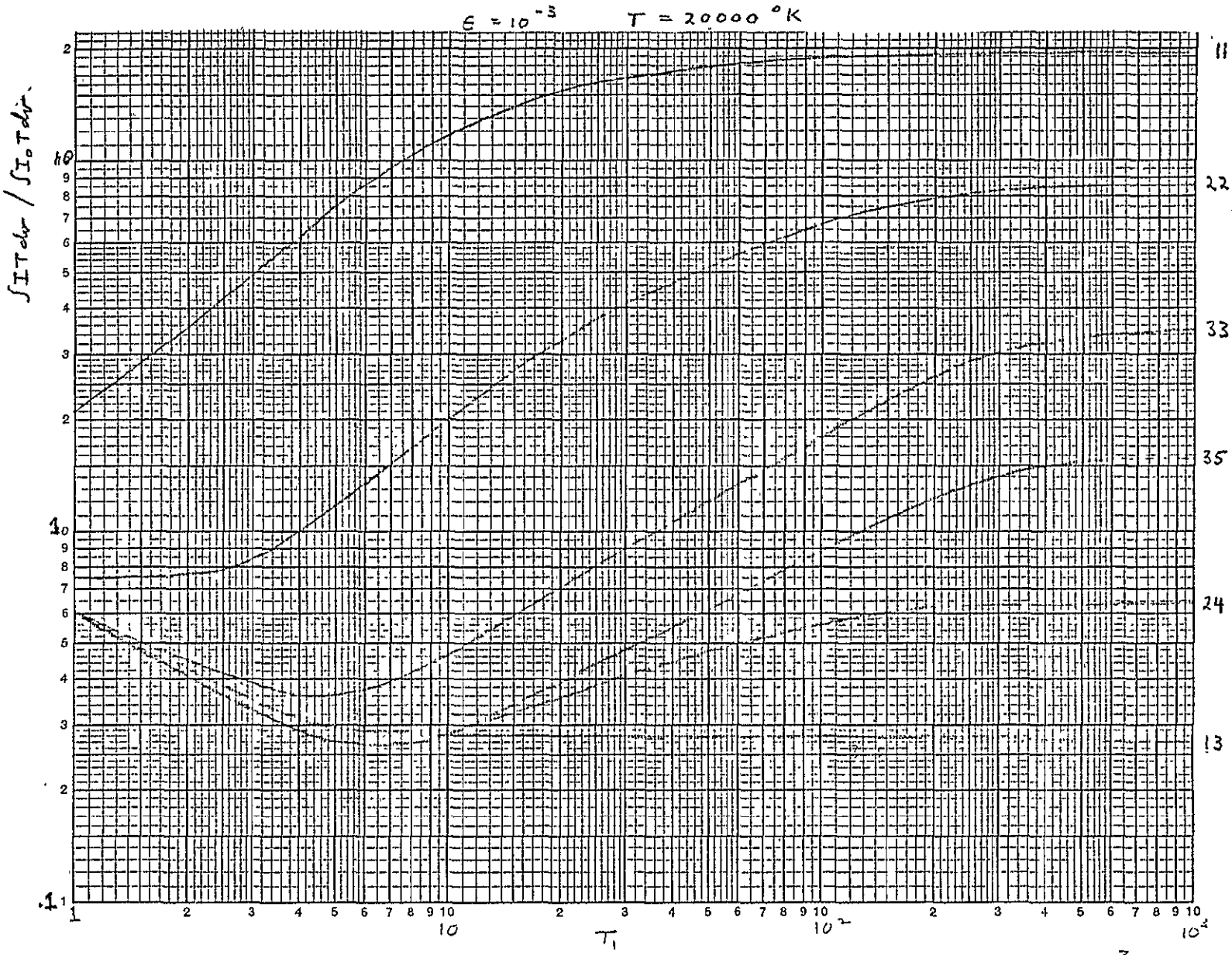

Figure III.B.6 Total Transmitted Line Intensity with Respect to Continuum for $\epsilon = 10^{-3}$. Curves are labeled with negative exponent values of η and i^*.

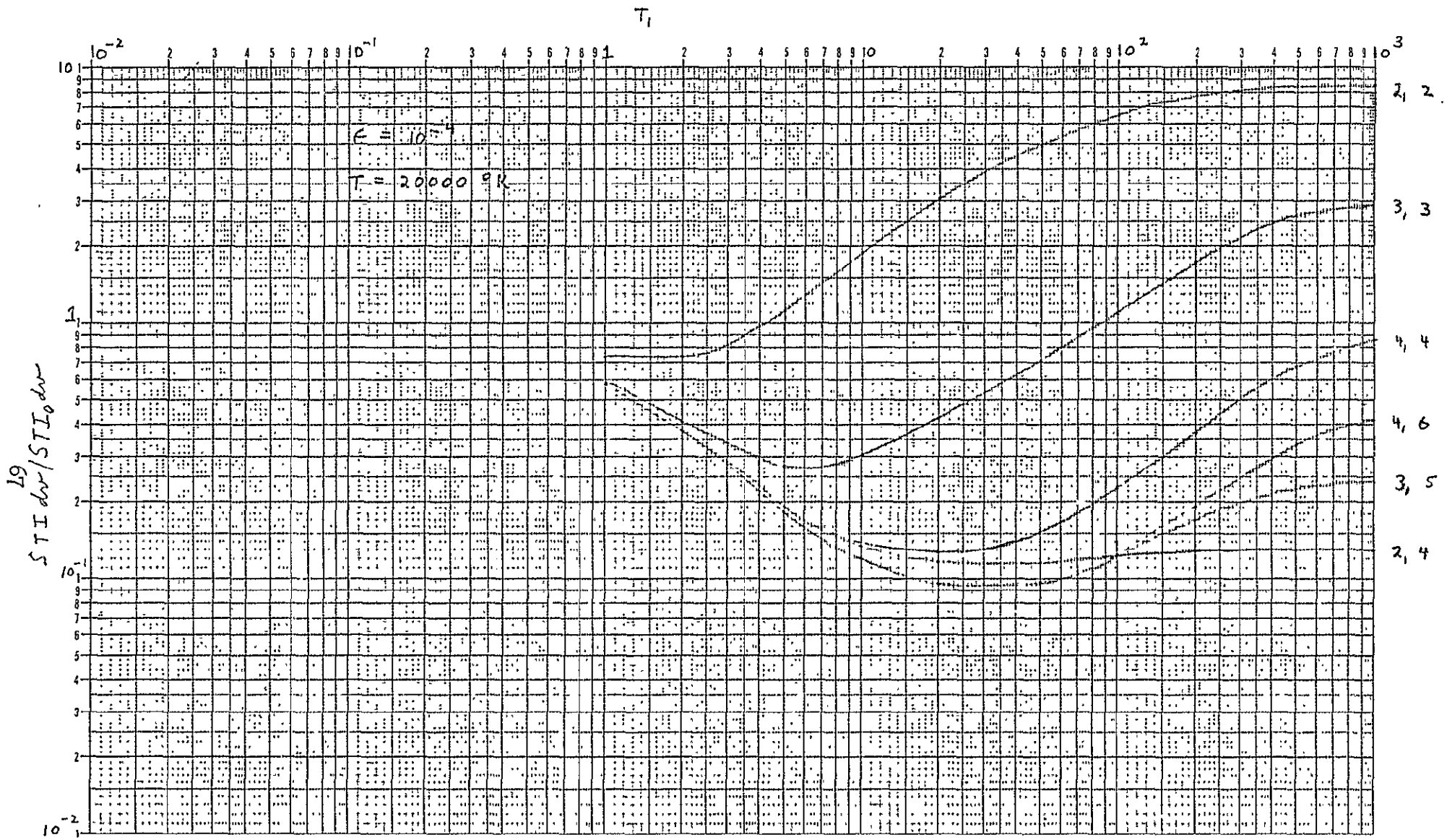

Figure III.B.7 Total Transmitted Line Intensity with Respect to Continuum for $\epsilon = 10^{-4}$. Curves are labeled with negative exponent values of η and i^*.

III. C. Electron Temperatures and Densities

The maximum flare D_3 intensities are about 1.2 times the normal background continuum. For each electron temperature and density we ask whether the corresponding values of ϵ, η and i^* will give line profiles yielding transmitted filter intensities greater than the continuum. In order to obtain an absolute D_3 intensity greater than the continuum with a layer no thicker than several thousand kms, n_e must be at least 10^{11}. The following temperatures, densities and optical thicknesses provide sufficient intensity: $n_e = 10^{13}$, $T = 20000\ ^oK$ - $40000\ ^oK$, $t_1 = 0$ - 2; $n_e = 10^{12}$, $T = 20000\ ^oK$, $t_1 = 10$ - 10^3.

The maximum D_3 flux in the flare is approximately 3.4×10^6 ergs/cm^2/sec/Å at the sun. The transmitted intensity is 6.0×10^5 ergs/cm^2/sec. At 20000 ^oK the total D_3 line flux is .157 times the intensity or 5.3×10^5.

We cannot determine the maximum 304Å intensities due to the solarized condition of plates 24, 25, 26 and 34. On plate 26 the 100 contour is at 40 times the background continuum while on plate 34 it is about 140 times the background continuum. By examining various positions within the flare we can determine that the intensities in the flare at 15:57:05 have decreased about 75% from those at 15:54:00.

The 256Å line intensities on plate 26 have not solarized. If we assume the same ratio of increase from positions near the intensity 100 contour on the 304 contour map as on the 256 contour map we can estimate the 304Å central intensities. This yields a maximum 304Å flare intensity of 800 times background intensity.

We shall use a quiet sun background intensity in 304 of 8600 ergs/cm^2/sec/st or flux 2.2×10^7 ergs/cm^2/sec. We thus arrive at an approximate 304Å to D_3 flux ratio of 40. Using the intensity curves derived in R1 we can determine the temperatures and densities allowing for a 304Å/D_3 ratio between 20 and 60. We find the following acceptable ranges: $T = 3 \times 10^4\ ^oK$, $n_e = 10^{12}$ - 10^{13} cm^{-3}; $T = 4 \times 10^4\ ^oK$, $n_e = 10^{12}$ - 3×10^{12} cm^{-3}. In order to have the correct absolute intensities the following optical thicknesses are required: $T = 3 \times 10^4$, $n_e = 10^{12}$, $t_1 = .1$ - .3; $T = 3 \times 10^4$, $n_e = 10^{13}$, $t_1 = .1$ - .2; $T = 4 \times 10^4$, $n_e = 10^{12}$, $t_1 = .1$ - .3; $T = 4 \times 10^4$, $n_e = 3 \times 10^{12}$, $t_1 = .2$ - .5. Comparing these ranges with those consistent with the D_3 emission we find the most probable flare condition at the brightest point to be $T \sim 3 \times 10^4\ ^oK$, $n_e \sim 10^{13}$ cm^{-3} and $t_1 \approx .1$ - .2.

Further interpretation is underway.

References

Benson, R. and J. L. Kulander, "Reaction Rates for HeI and II. Solar Physics, 27, 305.

Coffee, H. E., Worldwide Data Center A, Report UAG-43, "Catalog of Observation Times of Ground-Based Skylab Coordinated Solar Observing Programs," May 1975.

Harvey, K, private communication, 1971.

Kulander, J. L., "Departures from the Solar Equation in an Optically Thin Nitrogen Gas," J.Q.S.R.T. 5, 253, 1965.

Kulander, J. L., "He Emission from acitve Solar Regions," - Final Summary Report, NASA Huntsville # NAS8-27988, LMSC/D354991, Oct. 1973. - R1 in this document

Kulander, J. L., "He Emission from Model Flare Layers," to appear in Solar Physics, 1976.

Linsky, J. L., et. al., "The Solar XUV Spectrum of HeII, preprint, 1976.

Ramsey, H. E., "High Resolution Study of the Solar Atmosphere," - Final Report, NASW - 1890, LMSC/ 695791, May, 1970.

Ramsey, H. E., et. al., "A Comparison of Flares and Prominences in D_3 and H-α Final Report, AFCRL-TR-75-0355, Aug. 1975.

Appendix A

ENERGY LEVEL MODEL

TABLE I

He I, II Energy Levels

He I - i = 1

			Energy (ev)	Wave Nos.
1	$1s^2$	^1S	0	0
2	1s2s	^3S	19.821	159850
3	1s2s	^1S	20.618	166272
4	1s2p	$^3P^0$	20.966	169081
5	1s2p	$^1P^0$	21.220	171129
6	1s3s	^3S	22.721	183231
7	1s3s	^1S	22.923	184859
8	1s3p	$^3P^0$	23.009	185559
9	1s3d	^3D	23.076	186096
10	1s3d	^1D	23.076	186099
11	1s3p	$^1P^0$	23.089	186204
12	1s4s	^3S	23.596	190292
13	1s4s	^1S	23.676	190935
14	1s4p	$^3P^0$	23.710	191211
15	1s4d	^3D	23.738	191439
16	1s4d	^1D	23.739	191441
17	1s4f	$^3F^0$	23.739	191447
18	1s4f	$^1F^0$	23.739	191447
19	1s4p	$^1P^0$	23.744	191487

He II - i = 2

1	1s	^2S	0	0
2	2s	^2S	40.8099	329179.57
3	2p	$^2P^0$	40.8091	329182.02
4	3s	^2S	48.3662	390140.76
5	3p	$^2P^0$	48.3664	390141.49
6	3d	^2D	48.3665	390142.64
7	4s	^2S	51.0113	411476.98
8	4p	$^2P^0$	51.0114	411477.28
9	4d	^2D	51.0115	411477.77
10	4f	$^2F^0$	51.0117	411477.95

TABLE II

He I, II Lines

He I

	Upper Level	Lower Level	Notation	λ(Å)	A_8 (10^8/sec)	f
	4	2	1	10830	.1022	.5391
	5	1	2 UV	584.4	17.99	.2762
	5	3		20582	.01976	.3764
	6	4	10	7065	.278	.0693
	7	5	45	7281	.181	.0480
	8	2	2	3889	.09478	.06446
	8	6		4.30+4	.0108	.896
D3 →	9	4	11	5876	.706	.609
	9	8		1.86+5	1.28-4	.111
	10	5	46	6678	.638	.711
	11	1	3 UV	537.1	5.66	.0734
	11	3	4	5016	.1338	.1514
	11	7		7.43+4	.00253	.629
	12	4	12	4713	.106	.0118
	12	8		21120	.0652	.145
	13	5	47	5049	.0655	.00834
	13	11		21132	.0459	.103
	14	2	3	3188	.0505	.0231
	14	6		12538	.00608	.0429
	14	9		19543	.00597	.0205
	14	12		1.09+5	.0505	1.21
	15	4	14	4472	.251	.125
	15	8		17002	.0668	.482
	15	14		4.39+5	4.16-5	.200
	16	5	48	4922	.202	.122
	16	11		19089	.0711	.647
	17	9		18688	.139	1.02
	17	15		1.43+7	6.01-10	.0033
	18	10		18699	.138	1.01
	18	16		1.67+7	4.34-10	.00253
	19	1	4 UV	522.2	2.46	.030
	19	3	5	3965	.0717	.0507
	19	7		15088	.0137	.140

TABLE II (Continued).

He I

Upper Level	Lower Level	Notation	λ(Å)	A (10^8/sec)	f
19	10		18560	.00277	.00858
19	13		1.81+5	5.78-4	.853
19	16		2.17+6	5.65-7	.024

He II

3	1	303.80	100.	.4162
4	3	1640.5	1.01	.01359
5	1	256.3	26.8	.07910
5	2	1640.4	3.59	.4349
6	3	1640.4	10.3	.6958
7	3	1215.1	.413	3.045-3
7	5	4687.0	.294	.03225
8	1	243.03	10.9	.02899
8	2	1215.1	1.55	.1028
8	4	4686.8	.491	.4847
8	6	4687.2	.056	.01099
9	3	1215.1	3.30	.1218
9	5	4686.9	1.13	.6183
10	6	4687.1	2.21	1.018

Appendix B
BASIC EQUATIONS

In the statistically steady state the rate equation describing the population n_i of the state i is

$$\sum_{j\neq i} (n_j P_{ji} - n_i P_{ij}) = \sum_j n_j P_{ji} = 0$$

$$P_{ii} = - \sum_{j\neq i} P_{ij}, \qquad \text{A.1}$$

where P_{ij} is the total transition rate from i to j per second per particle in the i state. In general, $P_{ij} = R_{ij} + C_{ij}$, where R_{ij} and C_{ij} represent the radiative and collisional transition rates respectively. We shall assume a Maxwellian distribution for the electrons and helium particles and since we also assume a known external radiation field, the transitions involving the continuum can be represented by a single term in Eq. A.1. We can characterize the system of linear equations A.1 by a matrix whose coefficients a_{ij} are equal to P_{ji}. In representing matrix elements and co-factors thereof, we shall always let the first subscript refer to the row and the second to the column. Because of the definition of the transition rate the subscripts of the P's will be reversed when substituted for the matrix elements a. The general solution of Eq. A.1 is

$$n_i = \lambda_m P^{mi} \; ; \qquad \lambda_m = \frac{N}{\sum_j P^{mj}} , \qquad \text{A.2}$$

where P^{mj} is the co-factor of the element $a_{mj} = P_{jm}$ in the coefficient matrix represented by the i equations of type A.1 and N is the total number of helium particles per cm^3. The matrix of coefficients has the property that the co-factor of all the elements in a column are equal, i.e. P^{mj} is independent of m.

When the medium becomes optically non-thin for certain frequencies the radiation field producing internal excitation and ionization for these frequencies is no longer merely the external radiation field but is partly dependent on the internal properties of the gas and must be determined from the radiative-transfer equation

$$\mu \frac{dI_\nu}{d\tau_\nu} = I_\nu - S_\nu, \qquad \text{A.3}$$

where $\cos^{-1}\mu$ represents the angle between the direction of propagation and the outward normal z and $\tau_\nu = \int k_\nu \, dz$, S_ν is the source function, k_ν is the linear absorption coefficient and I_ν is the specific intensity of the radiation. In LTE $S_\nu = B_\nu$, however in the non-LTE case S_ν must be specified in terms of microscopic processes. In terms of such processes the transfer equation governing the spectral line between upper level u and lower level I may be written as

$$-4\pi\mu \frac{dI_\nu}{dz} = [n_l B_{lu} \Phi_\nu h\nu - n_u B_{ul} \psi_\nu h\nu + 4\pi k_c] I_\nu - n_u A_{ul} j_\nu h\nu - 4\pi k_c S_c(T_e), \qquad \text{A.4}$$

where k_c represents the continuum absorption coefficient at frequency ν_o and S_c is the continuum source function. B_{lu}, B_{ul} and A_{ul} are the Einstein transition probabilities for absorption, stimulated emission and spontaneous emission. j_ν, ψ_ν and Φ_ν are the normalized emission, stimulated emission and absorption coefficients within the line defined such that

$$\int_0^\infty \Phi_\nu d\nu = \int_0^\infty \psi_\nu d\nu = \frac{1}{4\pi} \int_{4\pi} \int_0^\infty j_\nu d\nu \, d\omega = 1.$$

The continuum absorption coefficient is generally very small compared with the line absorption coefficient near the line center and will be neglected in determining the source function within the line. Using the standard relations between the Einstein coefficients and assuming $j_\nu = \Phi_\nu = \psi_\nu$, the source function becomes

$$S_{ul} = \frac{2h\nu^3}{c^2} \quad \frac{1}{[(g_u/g_l)(n_l/n_u)]-1} , \qquad \text{A.5}$$

where g represents the statistical weight. The minus one term in the denominator represents stimulated emissions.

In evaluating the radiative excitation rate R_{ij} for transitions between bound levels the line radiation field enters as

$$\int_0^\infty J_\nu(\tau)\ \Phi_\nu(\tau)\ d\nu \ = \ \bar{J}(\tau)$$

where

$$J_\nu(\tau) = \frac{1}{4\pi} \int_{4\pi} I_\nu(\tau,\mu)\ d\omega$$

is the mean intensity and $d\omega$ represents the solid angle. It is thus convenient to formulate the transfer equation in terms of J_ν rather than I_ν. It is now convenient to separate those components involving the unknown radiation field, J_{ul}, from the co-factors. This is done by expanding the determinant P^{ij} in terms of its co-factors Q^{ij}. Thus

$$P^{lu} = \sum_{k\neq l} P_{lk}Q^{kl} = P_{lu}Q^{ul} + \sum_{k\neq l\neq u} P_{lk}Q^{kl}$$

$$P^{ul} = \sum_{k\neq u} P_{uk}Q^{ku} = P_{ul}Q^{lu} + \sum_{k\neq u\neq l} P_{uk}Q^{ku}. \qquad \text{A.6}$$

Actually, J_{ul} may appear in many of the co-factors since the line u-l may fall in the ionization continuum of some other transition. The influence of J_{ul} as well as the line radiation in general on the bound-free radiative rates will be neglected. Using the standard relationship between the

Einstein coefficients, equation A.6, and remembering that $Q^{ul} = Q^{lu}$ and $A_{lu} = B_{lu} \int J_\nu \bar{\Phi}_\nu d\nu$ the source function may be written as

$$S_{ul} = \rho_{ul} \frac{P^{lu}}{P^{ul}} = \frac{\int_{ul} J_\nu \bar{\Phi}_\nu d\nu + \epsilon B + \zeta}{1 + \epsilon + \eta} \qquad \text{A.7}$$

where B is the Planck function

$$B_\nu(T_e) = \rho_{ul} \frac{C_{lu}}{C_{ul}}$$

$$\epsilon = \frac{C_{ul}}{A_{ul}} \qquad \rho_{ul} = \frac{2h\nu^3}{c^2} \frac{g_l}{g_u}$$

$$\zeta = \rho_{ul} \frac{1}{A_{ul} Q^{ul}} \sum_{k \neq u \neq l} P_{lk} Q^{kl} \qquad \text{A.8}$$

$$\eta = \frac{1}{A_{ul} Q^{ul}} \sum_{k \neq u \neq l} P_{uk} Q^{ku}.$$

The terms entering the numerator of Eq. A.7 each represent a method of populating the upper level from the lower level. The first term represents direct radiative excitation, the second direct collisional excitation and the third any combination of radiative or collisional processes involving one or more intermediate levels in going from the lower to the upper level. The denominator, on the other hand, consists of terms indicating transition paths from the upper to the lower level. All the terms are normalized with respect to A_{21}. The first term represents direct radiative de-excitation, the second direct collisional de-excitation and the third any indirect process going from the upper to the lower state.

The problem remains of finding a $J_\nu(t)$ to use in evaluating the source function. One method we shall adopt is the general procedure of Thomas and Zirker (1961) in employing the Eddington transfer equation and replacing the integral in equation (A.2) by a standard quadrature. Specifically, an n-point Gaussian quadrature, as discussed by Avrett and Hummer (1965), is employed over the central line region where significant transfer of radiation occurs. As they point out, the Gaussian quadrature proves much more accurate than the Hermite-Gauss quadrature for finite layers.

The transfer equation for each quadrature frequency ν_i, assuming negligible continuous opacity, is

$$\frac{d^2 J_i^*}{dt^2} = x_i^2 \left[J_i^* - \frac{\Sigma a_i J_i^* + \epsilon + i^*}{(1 + \epsilon + \eta - \delta i)} \right] \qquad \text{A.9}$$

where

$$x_i = \sqrt{3}\varphi_i, \quad \varphi_i = \varkappa_L(\nu_i)/\varkappa_0 .$$

$\varkappa_L$ and $\varkappa_0$ are the line and line center absorption coefficients and a_i are the weight coefficients of the Gauss quadrature.

The solution of equation (A.9) regarding ϵ, η and i^* as constants for a layer of optical thickness t_1, is

$$J_i^* = \bar{\omega} \sum_\alpha \frac{L_\alpha}{1 - k_\alpha^2/x_i^2} \left[e^{-k_x t_i} + e^{-k_\alpha (t_1 - t)} \right] + \Delta + \bar{\omega} \sum_\alpha \frac{F_\alpha e^{-k_\alpha (t_1 - t)}}{1 - k_\alpha^2/x_i^2} \qquad \text{A.10}$$

where

$$\Delta = \frac{\epsilon + i^*}{\epsilon + \eta - \delta i} \qquad \text{A.11}$$

and

$$\bar{\omega} = [(1 + \epsilon + \eta - \delta i)]^{-1} \qquad \text{A.12}$$

The k_α are given by

$$\sum_{i=1}^{n} \frac{\bar{\omega} a_i}{1 - k^2/x_i^2} = 1 \quad . \tag{A.13}$$

Application of the boundary condition, which requires no incident radiation on the top surface of the layer, and an intensity WB_r on the bottom surface (W is a dilution factor) yields the following expression for the integration constants L_α and F_α

$$\sum_\alpha \frac{\bar{\omega} L_\alpha}{1 - k_\alpha/x_i} \left[1 + \frac{1 - k_\alpha/x_i}{1 + k_\alpha/x_i} e^{-k_\alpha t_1} \right] = -\Delta + WB_r/B_e \tag{A.14}$$

$$\sum_\alpha \frac{F_\alpha}{1 - 1_\alpha/x_i} \left[1 - \frac{(1 - k_\alpha/x_i)}{(1 + k_\alpha/x_i)} e^{-k_\alpha t_i} \right] = W B_r/B$$

The line source function (equation (A.7) then becomes,

$$S^* = \bar{\omega} \sum_\alpha L_\alpha \left[e^{-k_\alpha t} + e^{-k_2(t_1 - t)} \right] + \Delta + \bar{\omega} \sum_\alpha F_\alpha e^{-k_\alpha (t_1 - t)} \tag{A.15}$$

The emergent intensity $[I_\nu(0, \mu)/B] = I_\nu^*(0, \mu)$ from the surface of the layer at angle $\cos^{-1}\mu$ with respect to the normal, is

$$I_\nu^*(0, \mu) = \int_0^{t_1} \varphi_\nu S_L^* \exp\left(- \int_0^t \varphi_\nu \, dt/\mu \right) dt/\mu \quad . \tag{A.16}$$

With S_L given by equation (A.15) and φ_ν a constant with depth, the intensity becomes

$$I_\nu^*(0, \mu) = \bar{\omega} \varphi_\nu \sum_\alpha L_\alpha \left\{ \left[\frac{1 - e^{-[k_\alpha + (\varphi_\nu/\mu)]t_1}}{(\varphi_\nu + k_\alpha \mu)} + \frac{e^{-k_\alpha t_1} - e^{(-\varphi_\nu t_1/\mu)}}{(\varphi_\nu - k_\alpha \mu)} \right] \right\}$$

$$+ \Delta \left(1 - e^{-\varphi_\nu t_1/\mu} \right) \quad . \tag{A.17}$$

This equation is the basic equation from which the total integrated line radiation will be obtained.

When the optical thickness exceeds unity, a self-reversed or apparent absorption region develops near the line center resulting from the rapid increase in the source function with depth in the layer.